Final Report

March 1978

NASA CR-145380

EVALUATION OF A NEAR-INFRARED PHOTOMULTIPLIER FOR AIRBORNE LIDAR APPLICATIONS

By: WM. E. EVANS

Prepared for:

NATIONAL AERONAUTICS AND SPACE ADMINISTRATION
LANGLEY RESEARCH CENTER
HAMPTON, VIRGINIA 23365

NASA
National Aeronautics and
Space Administration

CONTRACT NAS1-15114

SRI Project 6919

333 Ravenswood Avenue
Menlo Park, California 94025 U.S.A.
(415) 326-6200
Cable: STANRES, Menlo Park
TWX: 910-373-1246

SRI International

Final Report *March 1978*

EVALUATION OF A NEAR-INFRARED PHOTOMULTIPLIER FOR AIRBORNE LIDAR APPLICATIONS

By: WM. E. EVANS

Prepared for:

NATIONAL AERONAUTICS AND SPACE ADMINISTRATION
LANGLEY RESEARCH CENTER
HAMPTON, VIRGINIA 23365

National Aeronautics and
Space Administration

CONTRACT NAS1-15114

SRI Project 6919

Approved by:

CHARLES J. SHOENS, *Director*
Systems Techniques Laboratory

DAVID A. JOHNSON, *Executive Director*
Electronics and Radio Sciences Division

Copy No. .....

333 Ravenswood Avenue • Menlo Park, California 94025 • U.S.A.

CONTENTS

"Page missing from available version"

ILLUSTRATIONS

TABLES

I SUMMARY

A state-of-the-art, near-infrared-sensitive photomultiplier tube was procured, set up, and operated in a laboratory environment for six weeks. The VPM-164A tube was maintained continuously at a temperature of -20°C while evaluation tests were conducted that were designed to emphasize features of particular importance to its possible use in a high-performance airborne stratospheric lidar. The principal findings are summarized in the following:

(1) Cathode quantum efficiency was measured as 4.3% at λ = 1.06μm and remained stable during the subsequent tests.

(2) The dark count was approximately 22,000 photocathode events per second at delivery and had dropped to an average level of about 19,000 counts/second by the end of the test period.

(3) The analog output drive capability is low by comparison with most standard photomultipliers. The curve of anode current versus short-pulse light power input is linear up to anode currents of about 0.2 mA. Linearity decreases moderately up to anode currents of 2 mA. Severe but well-behaved limiting occurs for peak anode currents above 2 mA.

(4) Dynamic gain control can be accomplished without signal degradation by supplying modulation voltage to selected dynode electrodes. However, appreciably more modulation voltage is required than for 7265 and 56TVP tube types tested previously. In excess of one decade of gain control per stage can be obtained relatively easily, and control stages can be cascaded for additional range.

(5) A Signal-induced noise effect is quite pronounced at low light levels (most noticeable in the photon-counting regime). Its magnitude is such that the effect should be characterized more completely so that suitable corrections can be included in computational procedures.

(6) The special gallium phosphide first dynode is not as effective in sharpening the single-electron-pulse amplitude distribution as had been expected. This in turn may make it slightly more difficult to obtain reliable absolute amplitude calibration when using photon-counting circuitry.

(7) Severe transient overloads such as might be generated by lidar backscatter from nearby dense cloud do not appear to cause any gross problems, either in the form of permanent damage or in the analog signal waveform for ranges beyond the cloud.

(8) Maximum permissible dc current limits for both cathode and anode are low enough that optical shuttering and/or severe gain gating should be included in the lidar receiver to prevent possible permanent loss of cathode sensitivity during sustained viewing of bright clouds.

(9) While the tube must be kept cold most of its life, a relatively small, low-power thermoelectrically cooled housing is commercially available to fit the tube. In addition, it has been found that occasional short periods (up to one or two hours) at room temperature can be safely tolerated. These two factors combine to make the tube cooling requirements for field applications appear appreciably less formidable than would otherwise be the case.

(10) The evaluation tube was obtained in a special reduced-diameter shell that is not normally advertised by the manufacturer. While it is now known that a standard-diameter shell could fit into the cooled housing described above, the reduced thermal lag and closer access to the cathode remain as attractive features for the reduced-size option.

It is concluded that if carefully used, the VPM-164A photomultiplier should make an excellent and probably unsurpassed detector for use in an airborne neodymium stratospheric lidar.

II INTRODUCTION

NASA is planning several programs that will require lidar measurements of the amount and distribution of stratospheric aerosols at heights above 20 km. Use of a high-altitude aircraft as a platform for the upward-looking optical probe offers attractive advantages not only in reduced path attenuation but also in placing observation equipment in the right location at the right time. This feature will be particularly attractive in providing corroborative data to support the several satellite-borne stratospheric aerosol experiments planned for the near future.

On the other hand, use of such a mobile platform demands a very high-performance lidar to minimize the integration time required to attain useful measurement accuracies, and places some practical restrictions on the equipment that can be carried.

The several advantages of using a neodymium laser in the lidar transmitter have been outweighed in the past by the low sensitivity and high noise levels of available photon detectors at the 1.06-μm infrared wavelength. As pointed out in a previous design study (Ref. 1),* over the past few years very significant, almost phenomenal advances have been made in infrared detector performance, primarily as a result of well funded, defense-related, non-lidar programs.

One product of such research had previously been identified as a promising candidate for possible use in a neodymium lidar receiver. It was the Varian type VPM-164A photomultiplier tube (PMT), a sophisticated device combining very-high-vacuum technique with modern semiconductor technology to achieve both low noise and quantum yields of several percent at 1.06 μm wavelength.

---

*References are listed at the end of the report.

The present study was initiated to procure one of these tubes and to test it with particular emphasis on those characteristics that might be affected by the uniquely large dynamic range of the atmospheric lidar signature and that are not included in a tube specification.

Considerable experience in identifying and coping with a wide variety of spurious effects in more conventional photomultipliers provided the necessary background for this study, which was to include performance checks in both the analog and photon counting mode. The essence of lidar probing is time-resolved signature analysis, and the best currently known method of amplitude calibration for unknown stratospheric returns is to compare them to the much stronger signal returns received a few microseconds earlier from better known regions at lower altitudes. Hence, there is special incentive to search for effects where light signals received from one range can modify those received from another range.

III TUBE EVALUATION TESTS

A. Mechanical, Thermal, and Magnetic Considerations

One of the most obvious objections to the use of the VPM-164A PMT in an aircraft field program is the manufacturer's stipulation that the tube always be maintained below usual room temperature (and preferably below -20°C), whether operating or not, to prevent deterioration that could possibly void the warranty. (A tube specification and warranty is included in the Appendix.) To fully comply with this requirement a lidar receiver design must provide not only a refrigerated PMT housing but also some means for assuring essentially continuous power or coolant--a task that can be particularly annoying during immediate preflight or post-flight operations. For this reason, more time than could be justified for a laboratory evaluation alone was spent in arriving at a cooled housing design that would be compact enough to be easily removed from the lidar and transported to a reliable power source for storage. A commercially available thermoelectrically cooled housing that came close to meeting this requirement was the type TE-102 housing manufactured by Products for Research, Inc., Danvers, Massachusetts. It employs 6-volt Peltier cooling elements (45 watts drain) and could be simply modified to operate for short periods from an automobile battery.

However, the standard VPM-164A tube is 7.5 mm too large in diameter to fit into the standard TE-102 housing. Discussions with both manufacturers revealed that through relatively minor modifications to the standard products, both a smaller tube and a larger inside diameter for the housing could be supplied. The concessions required for the tube were (1) that it would have a metal seal-off protrusion at one side that would require protection during handling and would normally operate at high voltage (near cathode potential), and (2) the photocathode would be offset from the central axis of the tube shell. The concessions required for the housing were (1) that the inner surface of the cold cylinder

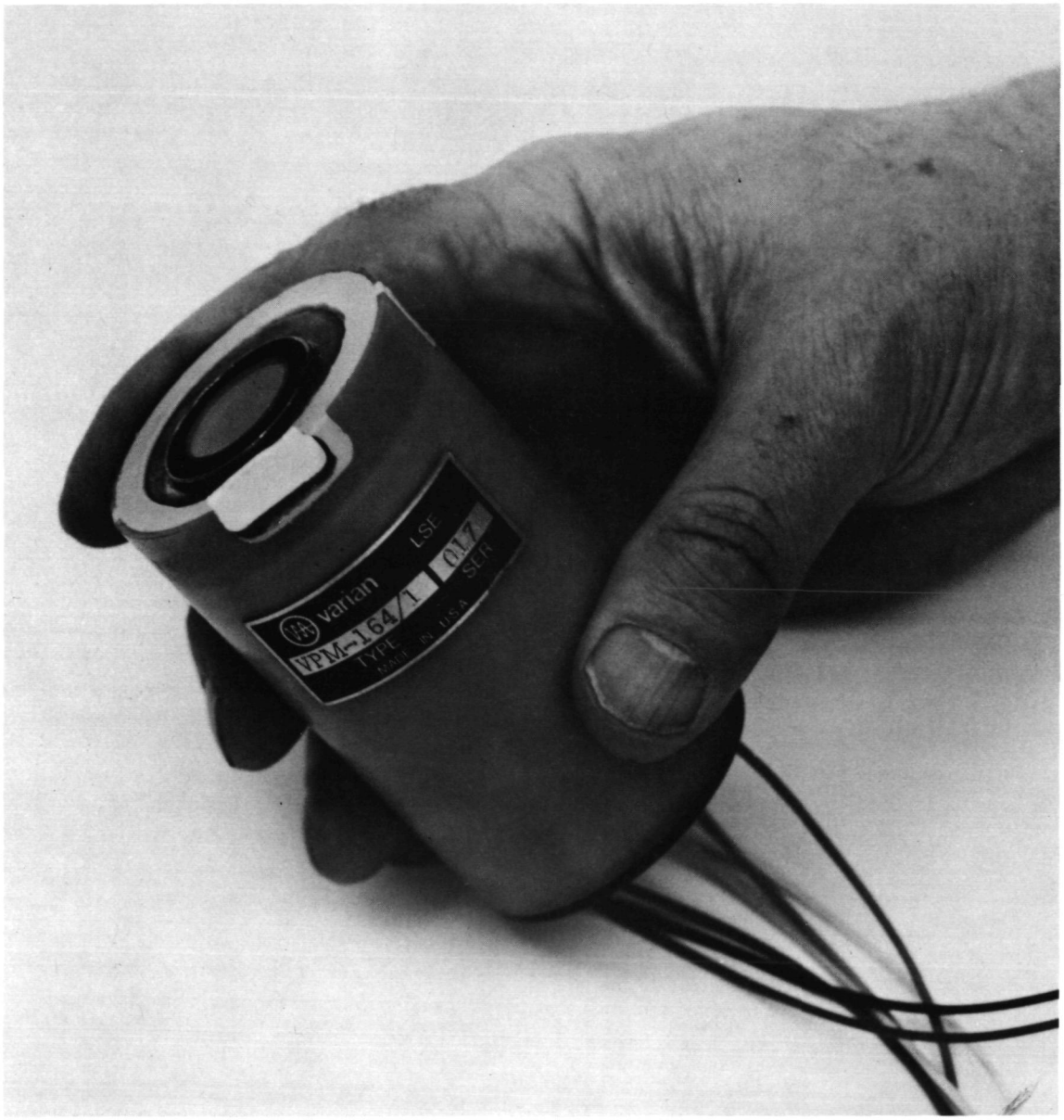

FIGURE 1 REDUCED-DIAMETER VERSION OF VPM-164A PHOTOMULTIPLIER

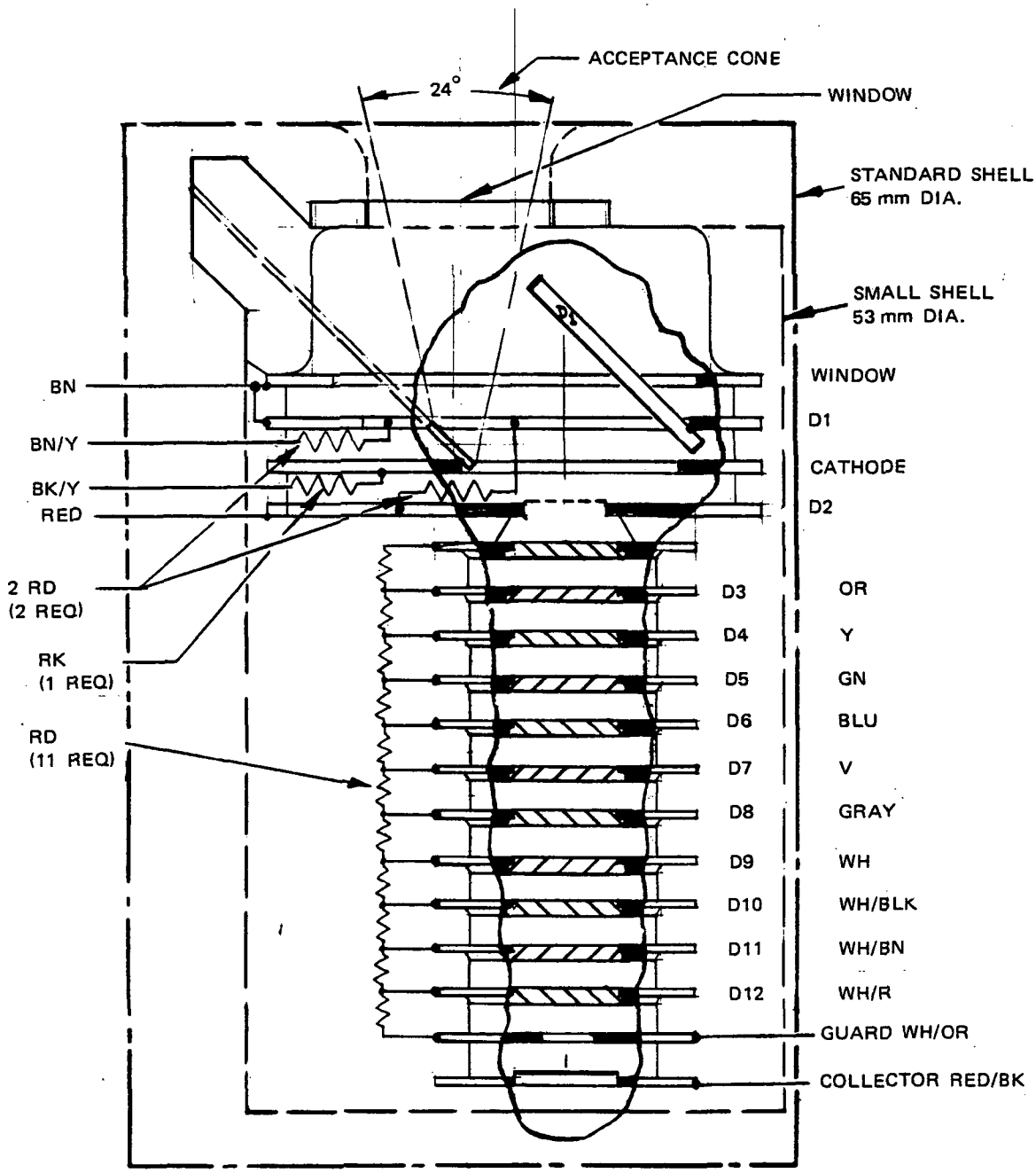

FIGURE 2 CUTAWAY VIEW OF VPM-164 GEOMETRY

would necessarily be at ground potential--in the standard model it could be operated at high voltage, (2) that full diameter access could be obtained from only one end, and (3) no magnetic shielding would be provided.

Fortunately these concessions do not conflict, and modified designs were ordered for both items with no effect on delivery schedules. Figure 1 is a photograph of one of the small (52.6 mm) diameter tubes. White tape covers the tubulation projection.

Figure 2 shows the main tube outline, both large and small shell designs, and a cutaway section depicting the internal structure. The drawing is a composite, derived partially from dimensions and descriptions supplied by the tube manufacturer and partially from visual examination of sample tubes. Thus, specific details may be in error or subject to change in future designs.

The space-saving measures were so effective that a standard VPM-164A tube would now fit into a modified housing. Conversely, the modified tube actually received would have fit into a standard unmodified housing, but this would not generally be true when manufacturing tolerances are taken into account.

Since, for the tube evaluation tests, it was desired to have easy electrical access to all of the tube elements, preliminary thermal tests were made on a standard TE-102 housing to determine whether the thermoelectric coolers would have sufficient capacity to keep up with heat conducted into the system by the relatively large number of connecting wires (16), and by any necessary structural members. The answer was a very marginal affirmative. It was found that the coolers must run continuously--i.e., at 100% duty cycle--to maintain the specified 40°C temperature differential between ambient air and the cold cylinder when one watt of heat is dissipated internally. The voltage divider resistor chain potted within the VPM-164A dissipates

0.077 watt at maximum applied voltage, and the heat conducted in through sixteen 28-gauge wires in parallel was calculated to be about 0.20 watt. Further, since the thermal conduction from the PMT cathode (the most important element to keep cool) to the fiberglass shell of the tube is so much poorer than the conduction through the wires, the cathode could be expected to stabilize at a temperature appreciably warmer than that of an encircling cold shell. Heat transfer calculations revealed that for a total temperature differential of 40°C the cathode-to-shell temperature differential should be approximately 5°C for the standard tube configuration, but only 0.5°C for the smaller-diameter modified tube because of the latter's lower thermal resistance from tube to shell. The 0.5°C figure was later verified by actual measurement on a defunct sample tube borrowed from the manufacturer.

The small-diameter tube design offers an additional advantage in that the metallic front element of the tube is exposed so that heat can readily be removed via a thermally conducting, electrically insulating washer. This permits the design of tube mounts that can provide still closer thermal coupling to the cathode area.

Figures 3(a) and 3(b) show two views of the tube mount and base assembly constructed at SRI for this project, and Figure 4 is a drawing of the same assembly showing the key dimensions. The machined aluminum cylinder holds the PMT with its cathode centered and provides a spring-loaded sliding fit into the cold cylinder. Between the front plate and the front PMT element is a 0.005-inch mica washer coated with thermal grease that provides good electrical insulation and fair thermal conductivity. In the light of the preceding discussion it now can be seen that adequate thermal characteristics could be obtained with either the cylindrical block or the flat plate acting alone, and a future design might achieve some simplification by eliminating one or the other. The rear portion of the assembly was fabricated from parts supplied by the housing manufacturer and normally used to make base assemblies for more

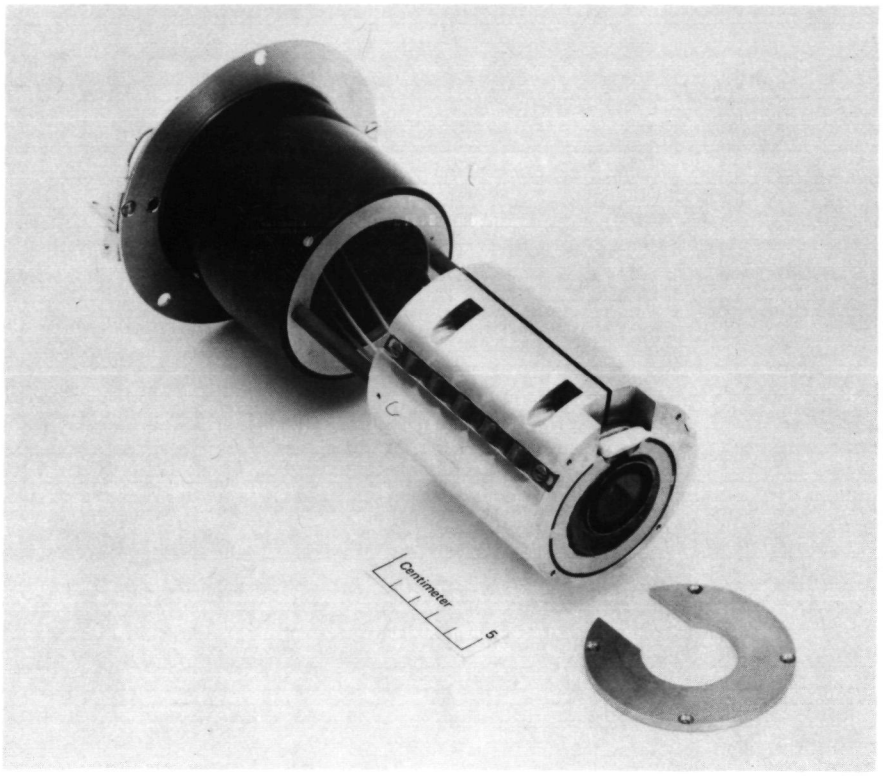

(a) FRONT VIEW WITH TUBE IN PLACE

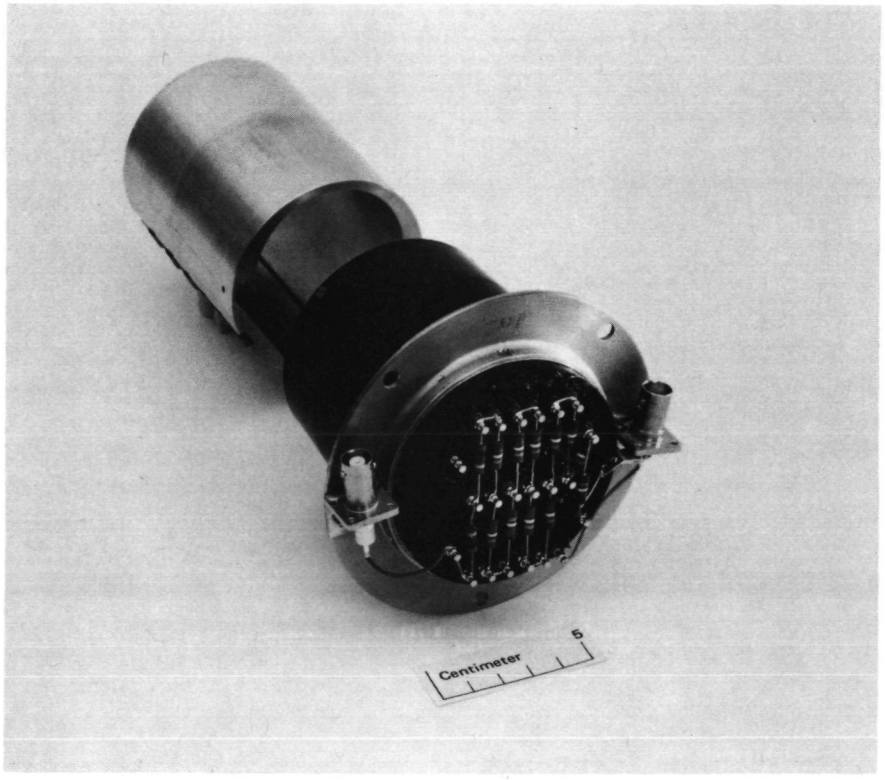

(b) REAR VIEW SHOWING EXTERNAL VOLTAGE DIVIDER

FIGURE 3 TUBE MOUNT AND BASE ASSEMBLY FOR VPM-164A PMT

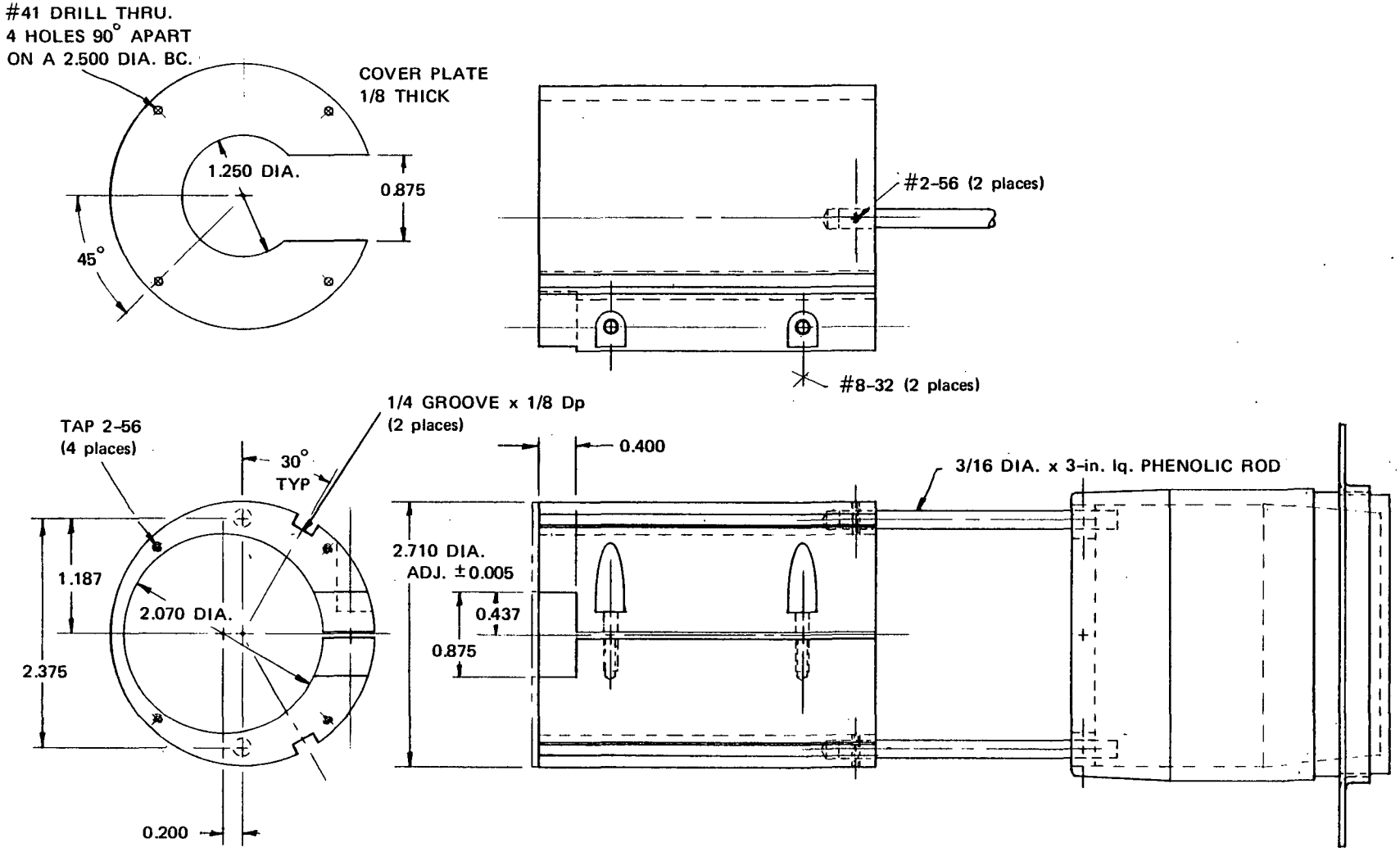

FIGURE 4 TUBE MOUNT AND BASE ASSEMBLY SHOWING KEY DIMENSIONS. All dimensions are in inches.

conventional phototubes. The design provides two O-ring hermetic seals to resist the tendency for moisture to be drawn into the housing by the internal negative pressure resulting from cooling. Light- and air-tight black nylon feed-through insulators were used to terminate the tube leads and to provide easily accessible mounting posts for an external voltage divider chain, bypass capacitators, and related components.

As mentioned previously, obtaining an enlarged cold-chamber diameter meant giving up both the electrostatic and magnetic shielding normally provided with the TE-102 housing. The static shielding sometimes required for glass PMTs is not needed for the metal and ceramic VPM-164A, since its acceleration fields are well controlled by a coaxial geometry and largely metal construction. Additionally, the closely coupled, venetian blind dynode structure of the VPM-164A provides performance that is also very insensitive to disturbance by external magnetic fields. This was verified by observing the dc output of the tube on an oscilloscope while subjecting the tube and cooled housing to the 60-Hz magnetic field from a TV degaussing coil. No interference was discernible ($\ll$ 10% of full amplitude) for any coil orientation, even though the field strength was on the order of 100 gauss rms, or approximately 400 times the average value for the earth's magnetic field. The operating gain during this test was $G = 10^6$.

B. Test Arrangement

Figure 5 is a block diagram showing the major items of test equipment used during the evaluation of the PMT, and Figure 6 is a photograph of the bench setup. To provide easy access to the tube base assembly and the voltage divider resistor string for wiring changes during the tests, the door containing a 120-cfm muffin fan at the rear of the housing normally was left open and room air was blown past the cooling fins by an external fan connected via the large canvas hose and a temporary cardboard plenum taped to the front of the housing. The external voltage divider resistors were each 1/10 the resistance of those built into the tube; that is, the basic interstage resistance value was 0.5

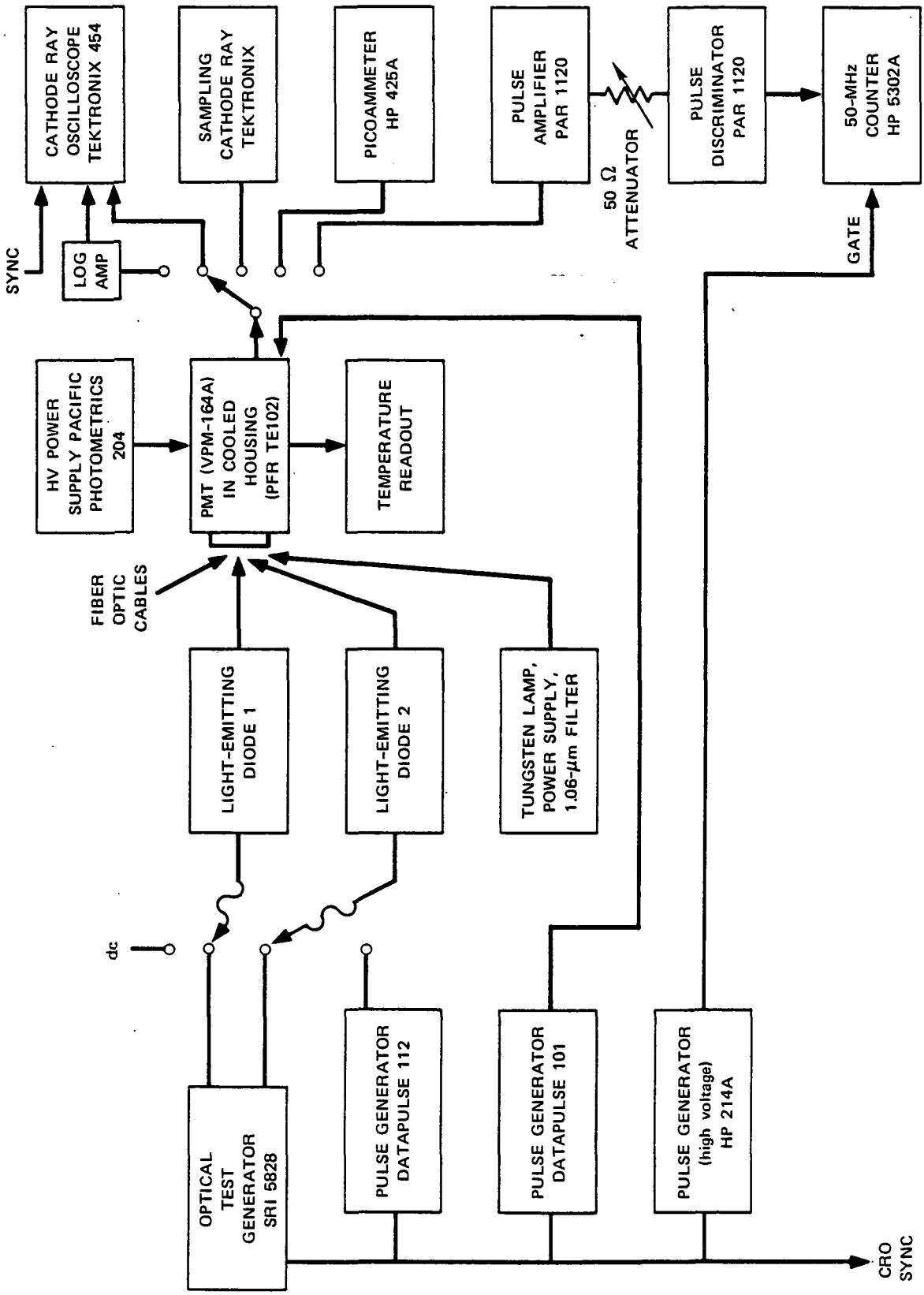

FIGURE 5 BLOCK DIAGRAM OF TEST ARRANGEMENT

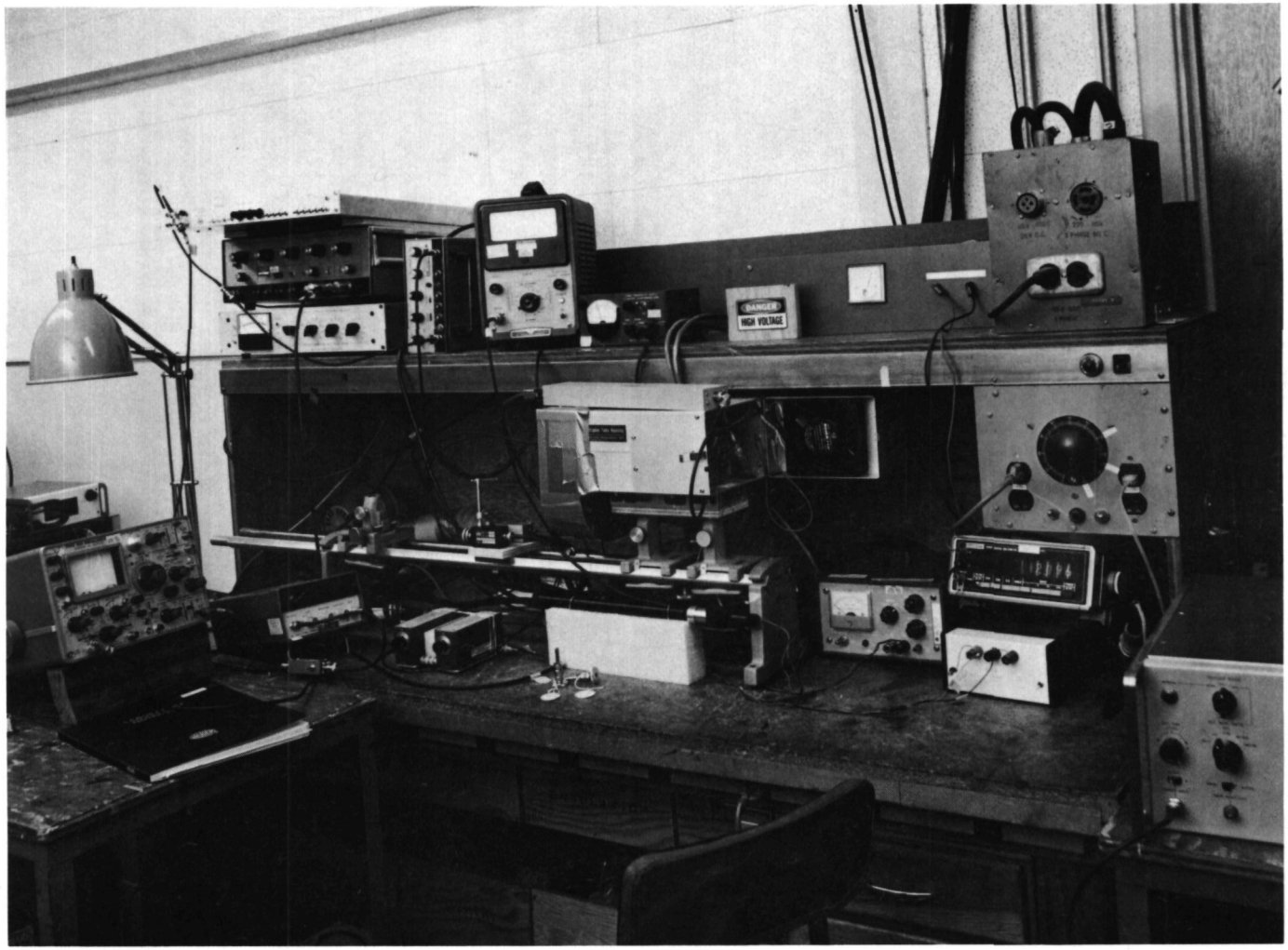

FIGURE 6 BENCH SETUP FOR PMT EVALUATION TESTS

megohm. Bypass capacitators (0.01 μF) were bridged across the last four resistors. Without them, severe distortion of high-amplitude analog signals results.

Figure 7 is a cross-sectional view of the cooled housing, PMT, and input fiber-optic coupling arrangement used for most of the tests. For direct imaging onto the photocathode, an alternate input assembly was available, consisting of a 50-mm lens and shutter and the plexiglass anti-frost cell normally supplied with the housing.

For most tests, light was supplied to the tube via one or more flexible plastic fiber-optic light guides fitted with universal end ferrules that mate to a variety of laboratory light sources. The light source most commonly used was a calibrated MV-10B light-emitting diode (LED) mounted in a small box and emitting at 660 nm. The optical test generator (flat unit with 1-3/4 inch front panel at the upper left of the bench setup) is an SRI-built piece of test equipment specifically designed for performing various diagnostic and calibration tests on lidar receivers. Both LED and gallium aluminum arsenide (GaAlAs) laser diode output transducers are used with the generator to provide repeatable and adjustable optical waveforms that closely simulate both lidar atmospheric returns and returns from flat targets. A special feature is that strong short-pulse signals are generated and distributed separately from the signals representing returns from distributed targets. These sources are combined only at the photo-cathode of the detector system under test so that any observed after-pulsing or paralysis effects are known to originate in the receiver, not in the generator.

The cooling system was operated continuously, with dc current to the thermoelectric units adjusted for the recommended value of 7.0 A. Temperature of the cold chamber was monitored via digital readout of the resistance of a calibrated "posistor" sensing element supplied as part of the housing. A separate reading of the housing interior temperature made at -20°C with a Fluke 80T-150 thermo probe checked the posistor readout to within 0.5°C.

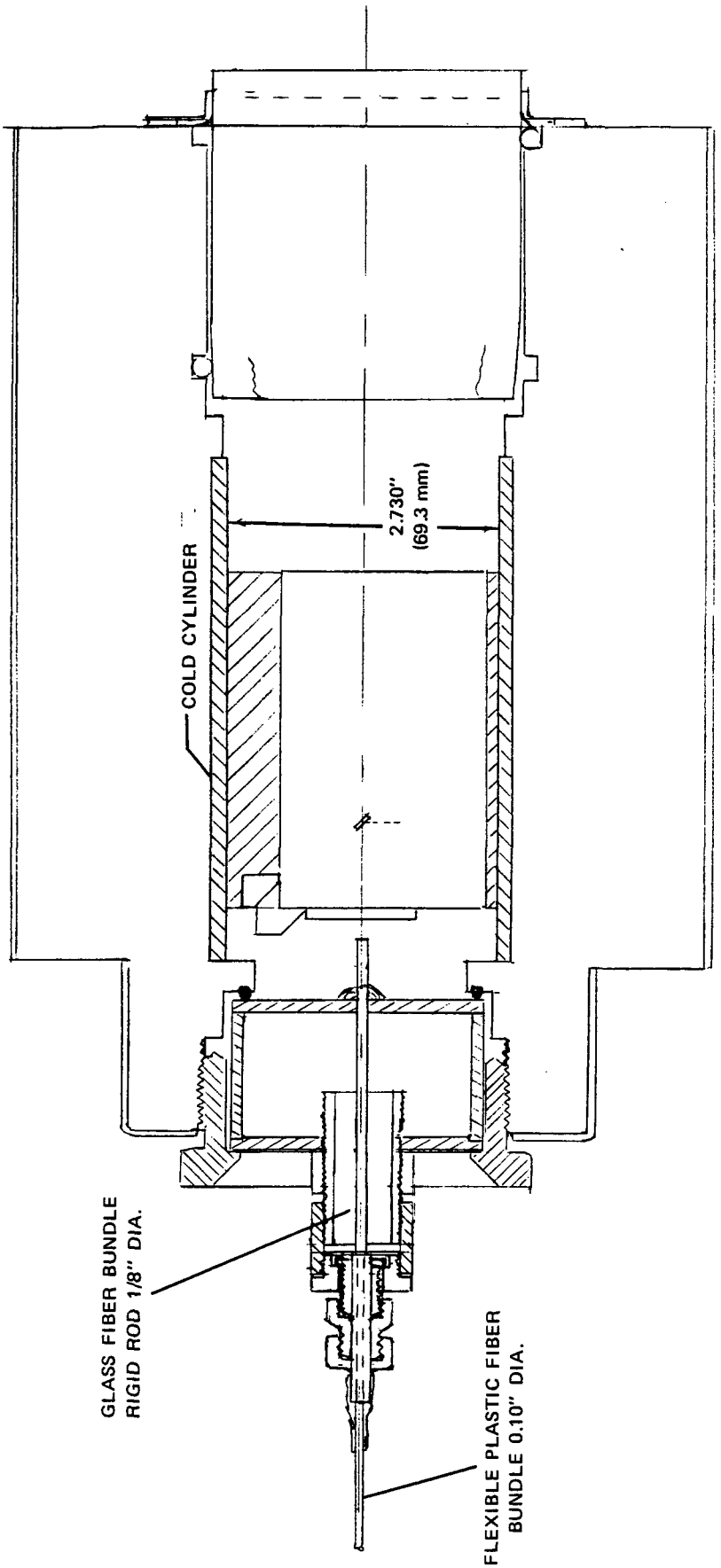

FIGURE 7 CROSS-SECTIONAL VIEW OF HOUSING, PMT, AND FIBER OPTIC INPUT COUPLING

Room temperature typically was within -1° and +2° of 22°C, being cooler in the morning and gradually warming in the afternoons. The lowest chamber temperature ever recorded was -21°C and the maximum excursion noted was 2.73° above that value. The most usual temperature readout was -19°.

C. Cathode Quantum Efficiency and Multiplier Gain

The author witnessed measurements of cathode quantum efficiency and multiplier gain made in the optical test laboratory of the manufacturer, Varian Associates, LSE Division, Palo Alto, California. The tests were made Friday afternoon February 3, 1978, just prior to delivery of the tube the following Monday morning. For all tests, the tube was in a large box, in a -20°C environment obtained by flowing dry nitrogen warmed from the liquid state. It was illuminated through a 4-by-5-inch-diameter quartz cylinder window by a 2-mm-diameter collimated beam from a Bausch & Lombe high intensity monochromator, Model 33-86-77. For the cathode tests the tube was operated as a diode with 300 volts between cathode and dynode No. 1. Output from the monochromator at various wavelengths was read from a calibration chart that had been derived from an Optronics Model 730 Radiometer. This radiometer constitutes the principal absolute standard for the laboratory. It is returned to the manufacturer in July each year for a calibration traceable to Bureau of Standards, and is also checked periodically against a 2870° K standard lamp maintained by Varian in a large permanent optical bench setup. Varian believes that its absolute sensitivity measurements are accurate to within ±5%.

The author witnessed measurements made at wavelengths of 530, 1060, and 1100 nm. The values agreed with points on the more extensive curve plotted earlier in the day and included in the Appendix.

For the gain measurements, the tube was operated with its internal voltage divider resistor string, and the overall voltages required to achieve stated ratios of anode-to-cathode currents were recorded. The measuring instrument was a Kiethley Model 414S Picoammeter and the

fundamental measurement was made at a gain of 10^3 (V = 820 volts) with 1.0 nA at the cathode and 1.0 μA at the anode. Subsequent gain measurements, in one-decade steps, were made by a step-and-repeat process of lowering the light to reduce the anode current to 0.1 μA, then raising the applied voltage to again achieve 1.0 μA. The results are given on the tube data sheet in the Appendix.

Independent gain measurements made later at SRI using both pulsed and dc light sources and using an external divider string (10 times the current of the internal divider) checked these values within 0.5%.

DC dark current was measured at G = 10^5 and is discussed further in Section III-F.

The next and last test was of the anode pulse amplitude distribution. These results are presented and discussed in Section III-H.

D. Amplitude Linearity

Figure 8 presents amplitude linearity characteristics measured for the PMT. Data were taken at λ = 660 nm, but should be valid for any wavelength because the curvature is undoubtedly due to space charge effects near the anode end of the tube. Data were read from an oscilloscope while the cathode was illuminated with pulsed light from the optical test generator. Signals with peak amplitudes below the 0-dB line had a fast rise waveform followed by an exponential decay with a time constant of 1 μs (slope = -4.343 dB/μs). Signals with levels above the 0-dB line were short spikes having a full width of 150 ns measured 30 dB below their peak amplitude. At the 0-dB level, which corresponded to a tube cathode current of 22 nA, measurements were made using both signal types. For references purposes, linear projections are drawn for each of the curves. The data show that departure from linearity begins at a tube output of about 10 mV (into 50 ohms), and that the output is 30 to 40% low for levels of 100 mV. This relatively low saturation level implies that additional gain will usually be required to achieve levels compatible with commonly used analog digitizers and transient recorders.

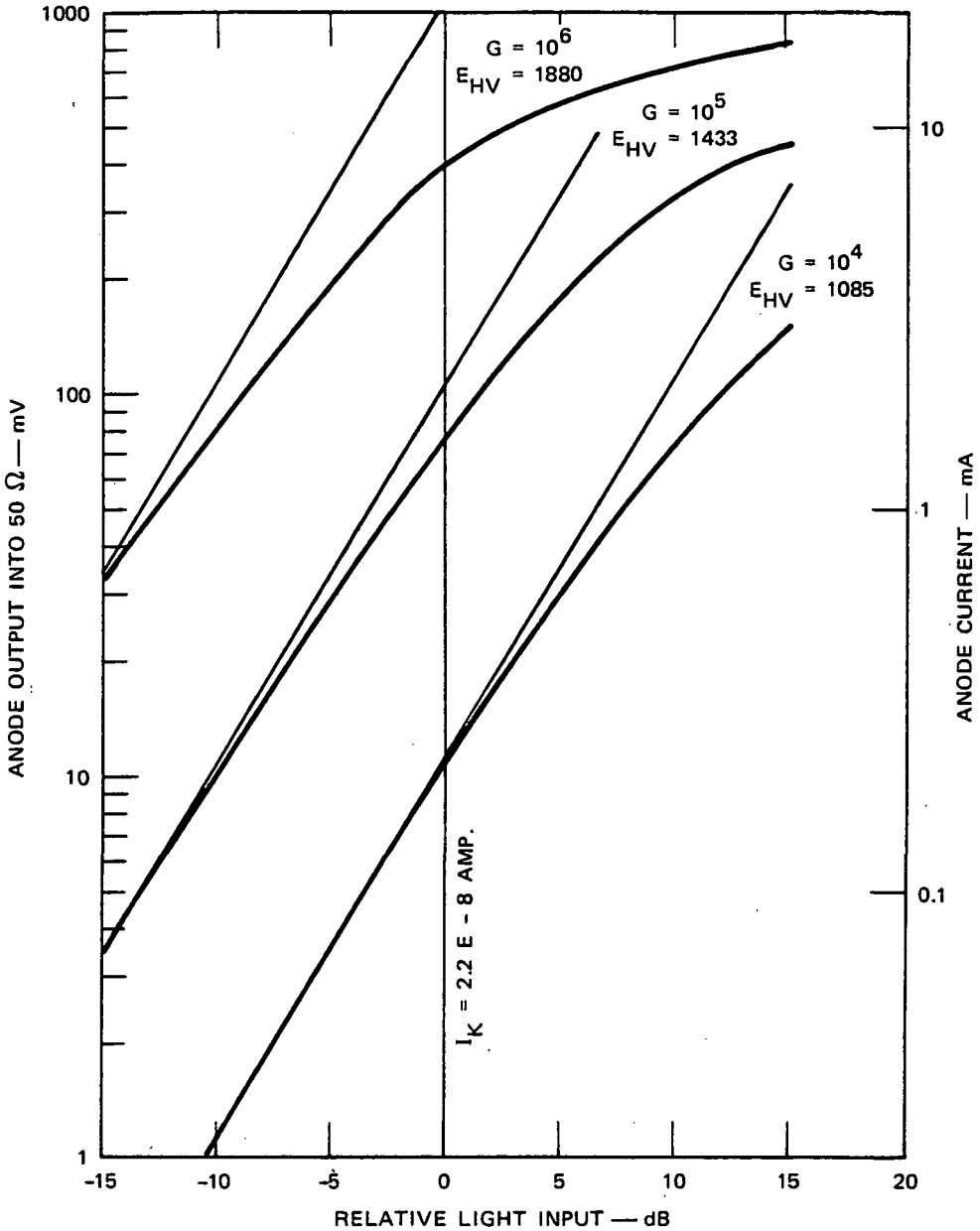

FIGURE 8 MEASURED AMPLITUDE LINEARITY CURVES — VPM-164A, SERIAL NO. 082, λ = 660 nm

E. Gain Control by Dynode Modulation

A procedure of achieving dynamic control of photomultiplier gain by applying relatively low-voltage control signals to one or more dynode electrodes was first used on the SRI Mark IV lidar in 1966 and has been successfully applied to virtually all SRI lidars since that time. Its use with an RCA 7265 tube in the Mark VIII Air Pollution Lidar was described in Ref. 2. The basic idea is to "detune" the potential of a selected dynode from its normal value midway between the potentials of its two nearest neighboring dynodes. As the potential is deviated from normal, the stage voltage and stage gain increase with respect to one neighbor and decrease with respect to the other neighbor. The rates of change of the two opposing gain effects are different, however, with the result that the overall gain of the two-stage combination varies over a hump-shaped characteristic that is fairly symmetric about its maximum.

The VPM-164A was found to follow the same general pattern just described, but the slope of its control characteristic was appreciably less steep than for other types of photomultiplier tubes measured previously. Figure 9 shows the measured control curve for the range of potentials from the potential of the next lower dynode to that of the next higher dynode and shows that over that range the gain can be reduced only to about 35% of its maximum. Curves for dynodes 3 and 5 are shown. Similar behaviour was found for other dynodes. Evidently the in-line, venetian-blind dynode structure is less susceptible to "detuning" than other tube geometries.

Since there was no evidence that the single-stage gain modulation limit had been reached, the test was extended so that the potential of the control dynode was carried "through" that of its next lower neighbor and on down to that of the n-2 stage. The resulting gain curves are given on Figure 10. They show that slightly over one decade of gain control can be achieved per stage, but that modulation voltages of from 100 to 150 volts are required, depending on the overall tube operating voltage.

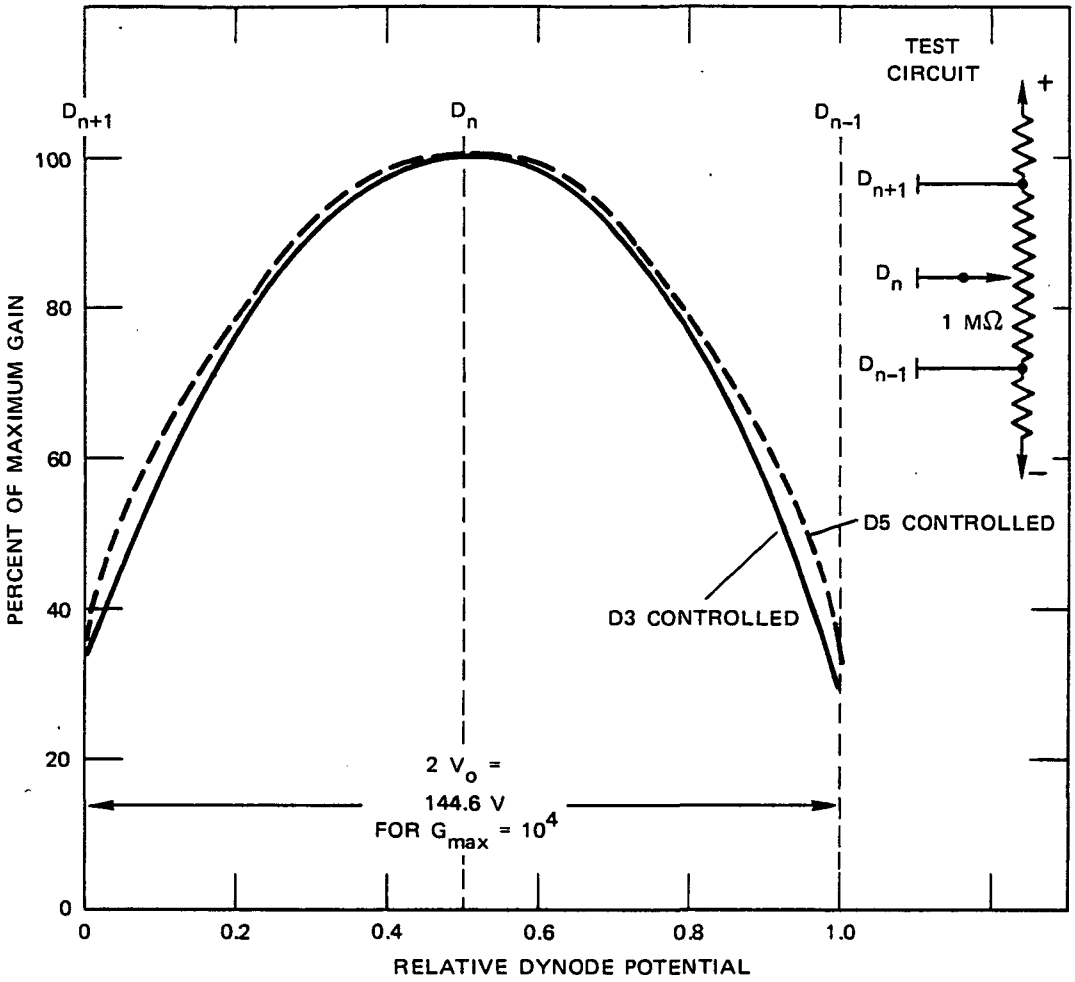

FIGURE 9 DYNODE GAIN-CONTROL CHARACTERISTICS — VPM-164A, SERIAL NO. 082, dc MEASUREMENTS

For modulation swings at least up to the level where the dynode potential reaches that of its nearest neighbor, gain control in successive odd-numbered or successive even-numbered stages can be cascaded without interaction, and the same modulation voltage can be coupled to each. A check for interaction was not made for the case where the modulation swing exeeds the normal stage voltage.

F. Internal Noise Levels

The traditional measure of detector internal "noise", the dark current, was measured before delivery as 5.0×10^{-10} A for a tube gain of 10^5 (see data sheet in Appendix). The dark current dropped slightly during the

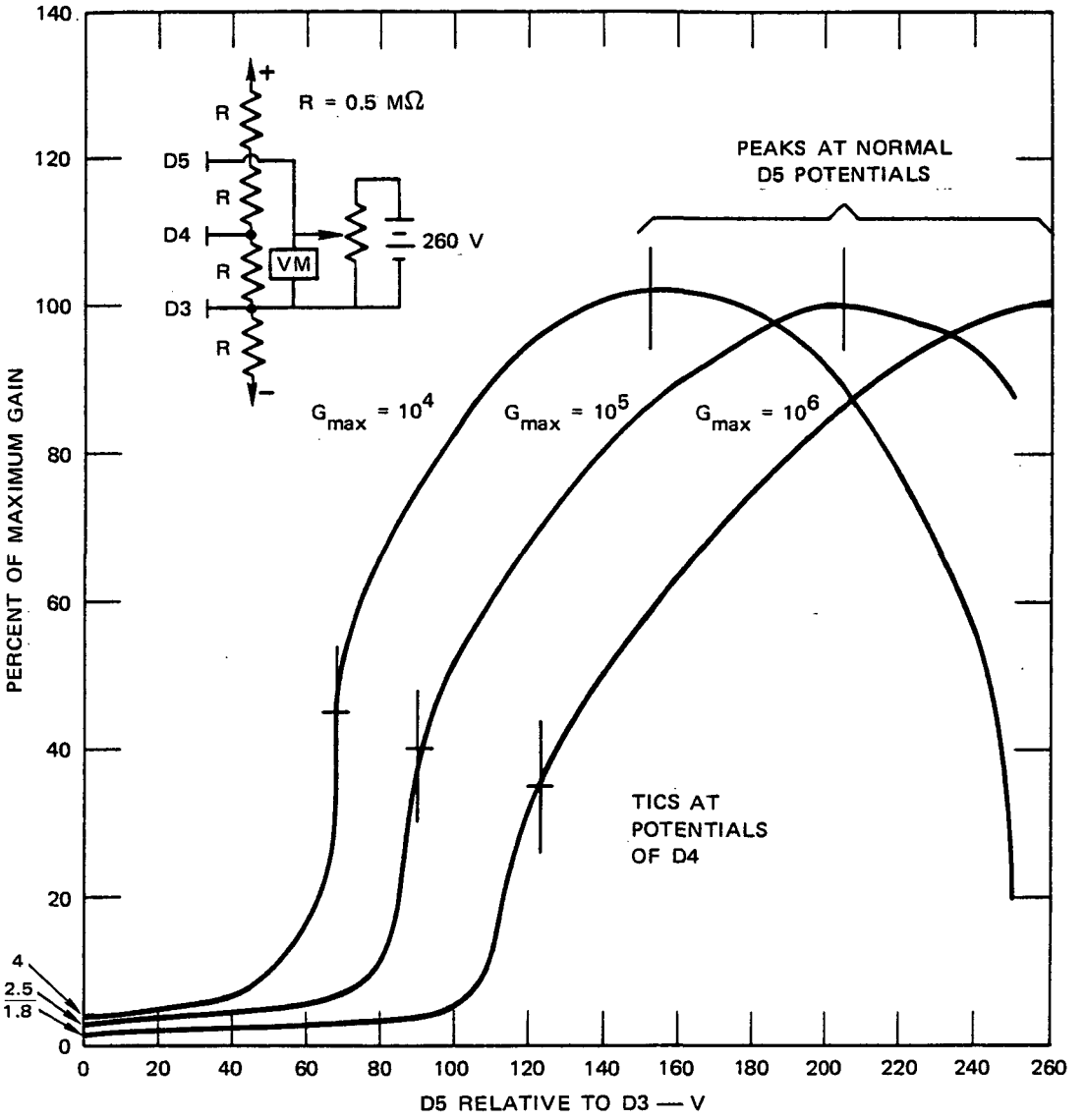

FIGURE 10 EXTENDED RANGE DYNODE GAIN CONTROL

first few days after delivery and was recorded as 3.4×10^{-10} A on February 8. If all of this current originated at the photocathode (which, fortunately, it does not) it would correspond to a cathode electron count rate of 3×10^9/s. The much more significant number is the dark count rate. While this number has precise meaning only when the threshold level and method of measurement are specified, it was comforting to note that a dark count rate of 22,435 counts/s (at T = -20°C) measured with factory equipment on February 3, before delivery, appears consistent with a dark count rate of 22,000/s recorded a month later at SRI using different equipment adjusted for a 75-μV threshold that is believed to correspond approximately to that used at the factory. Most of the SRI data were recorded with a threshold level of 333 μV referred to the anode ($G = 10^6$, R_L = 50 ohms).*

For this somewhat higher threshold, the average dark count slowly declined with time from about 3000/s in mid-February to about 1200/s in mid-March. On a Monday morning, after resting in the dark over the weekend, the count could go as low as 600/s. After just a few seconds of low-level illumination, it would rise to 1100 to 1200/s. By the end of a day's work the dark count would typically be 2500 to 3000/s. The lowest rate recorded for a 75 μV threshold was 19,000/s.

All of these rates are almost negligibly small when considered in relation to the range integration periods and probable total integration periods of an airborne lidar application.

G. Recovery from High-Level, Short-Pulse Exposures

1. Analog Mode

The tube manufacturer has established an upper limit of 100 nA average for the current that can be drawn from the photocathode without

---

* The Varian data are quoted in units of electron equivalents, e. The equivalent value in our nomenclature can be found by assuming that for an operating tube gain of 10^6, each photocathode event results in a normally distributed anode current pulse 20 ns wide (FWHM), as actually observed. The resulting voltage pulse across a 50-ohm termination would then have a peak value of 250 μV.

danger of desorption of critical cesium from the emitting surface of the semiconductor photocathode. For a typical one-joule, 0.3-m neodymium lidar, the clear-air atmospheric return from 1 km elevation with the lidar parked at sea level would generate a short-duration cathode current of 350 nA and thus should not be cause of concern at the cathode. The same signal would result in mild saturation at the anode (refer to linearity curves of Section III-D) even for tube gain as low as $G = 10^4$. Should the operating gain be higher and/or should nearby clouds be within the field of view, it is obvious that several decades of transient overloading can occur at the anode, and it is important to know whether weaker signals received from ranges beyond the stong return will be affected by the previous overload condition.

Using the optical test generator, a variety of tests were conducted in search of unusual performance following severe overloads, and none was found. Figure 11 shows logged analog waveforms for one such test. The ramp-shaped signal component simulating an atmospheric return was derived from an exponentially decaying current in a light-emitting diode. For all cases shown, this component was near or below the anode saturation level for the PMT. The short spike signal component was derived from a separate LED and is 24 dB (250 times) stronger than the peak of the atmospheric component.

It is seen that for all ranges beyond 200 ns after spike center there is no noticeable effect on the decaying analog waveform for any level of saturation during the spike. The occasional appearance of a shoulder on the trailing edge of the tall spike results from a known spurious characteristic of the spike generator and not from the detector.

In the laboratory, where the test signals could quickly be switched in and out while the results are being watched on an "A-B comparison" basis, the various instrumental anomalies were more easily ignored. With a higher degree of confidence than can readily be demonstrated photographically, the dynamic tests showed that the PMT was behaving rationally in the analog mode in spite of relatively severe input overloads.

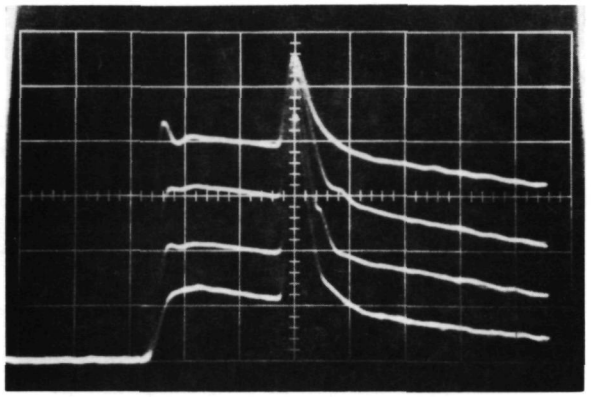

(a) SPIKE SIGNAL IS HELD CONSTANT AT 23 dB ABOVE SATURATION LEVEL. Simulated atmospheric return (exponential decay) is attenuated in steps of approximately 6 dB. PMT gain G = 10^5.

HORIZ = 200 ns/div VERT = 50 mV/div
= 5.7 dB/div

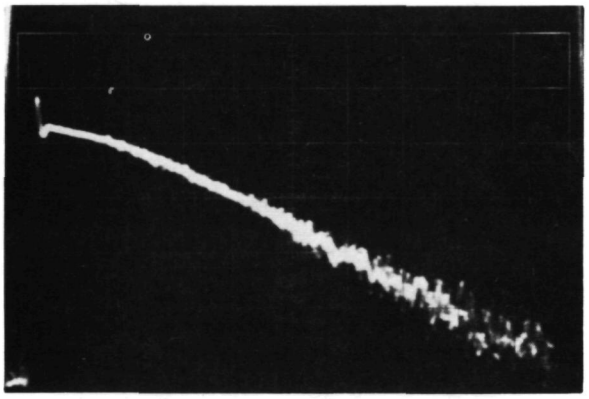

(b) EXCITING LIGHT DECAYS EXPONENTIALLY FROM SLIGHTLY ABOVE SATURATION LEVEL INTO PMT NOISE. PMT gain G = 10^6.

HORIZ = 0.5 μs/div VERT = 50 mV/div
= 5.7 dB/div

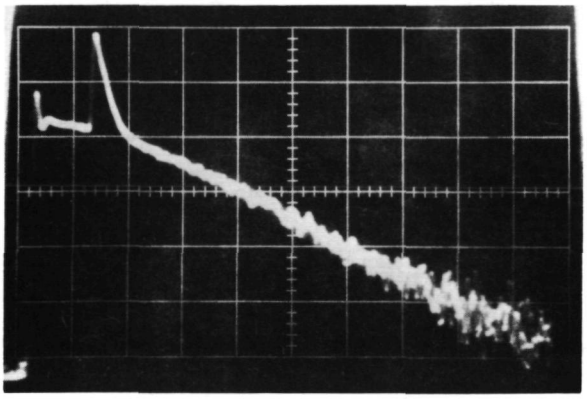

(c) SAME CONDITIONS AS (b) EXCEPT THAT SHORT SPIKE 33 dB ABOVE SATURATION LEVEL HAS BEEN ADDED.

HORIZ = 0.5 μs/div VERT = 50 mV/div
= 5.7 dB/div

FIGURE 11 ILLUSTRATIONS OF ANALOG RECOVERY FROM SHORT-PULSE OVERLOADS. For all cases, anode saturation level (2 mA) is four divisions up from bottom line. Positive overshoot at the leading edge results from a problem in the log amplifier.

2. Pulse-Counting Mode

Pettifer, Hunt (Refs. 3, 4, and 6) and others have reported on an annoying memory effect in photomultiplier tubes that has been termed "signal-induced noise." The effect is most noticeable when, after the complete termination of an exciting light flux, the tube output, expressed as an anode pulse count rate, does not immediately drop to the long-term background value but decays toward that limiting value over a period of tens or hundreds of microseconds. The same phenomenon affects the accuracy of time-resolved measurements made on a continuing light source, and the induced error may become significant for decaying signal waveforms such as those produced by a lidar. Pettifer's results were given for a type 56TUVP photomulitplier for a very low level of exciting light (10^{-13} W cm^{-2}) and for count rates more consistent with long-term integration in a ground-based lidar than for an airborne application.

To determine the gross magnitude of the signal-induced noise effect in the VPM-164A tube under test, the tube was irradiated with a rectangular light pulse of a magnitude sufficient to produce a photocathode current comparable to the maximum atmospheric return of a representative upward-looking, airborne neodymium lidar firing upward from an altitude of 10 km and adjusted for convergence 1 km above the lidar.

The system parameters assumed for this calculation were approximately those used for the design study of Ref. 1, and are given in Table 1.

The received power P_R incident on the photocathode from range R can be calculated from the lidar equation:

$$P_R \text{ (watts)} = \frac{U_T A_R c \beta T_o}{2R^2} \quad . \tag{1}$$

Figure 12, also taken from Ref. 1, plots solutions of the lidar equation for these assumed parameters. It shows that the maximum expected photocathode current at convergence will be about 10^4 photoelectron counts per microsecond.

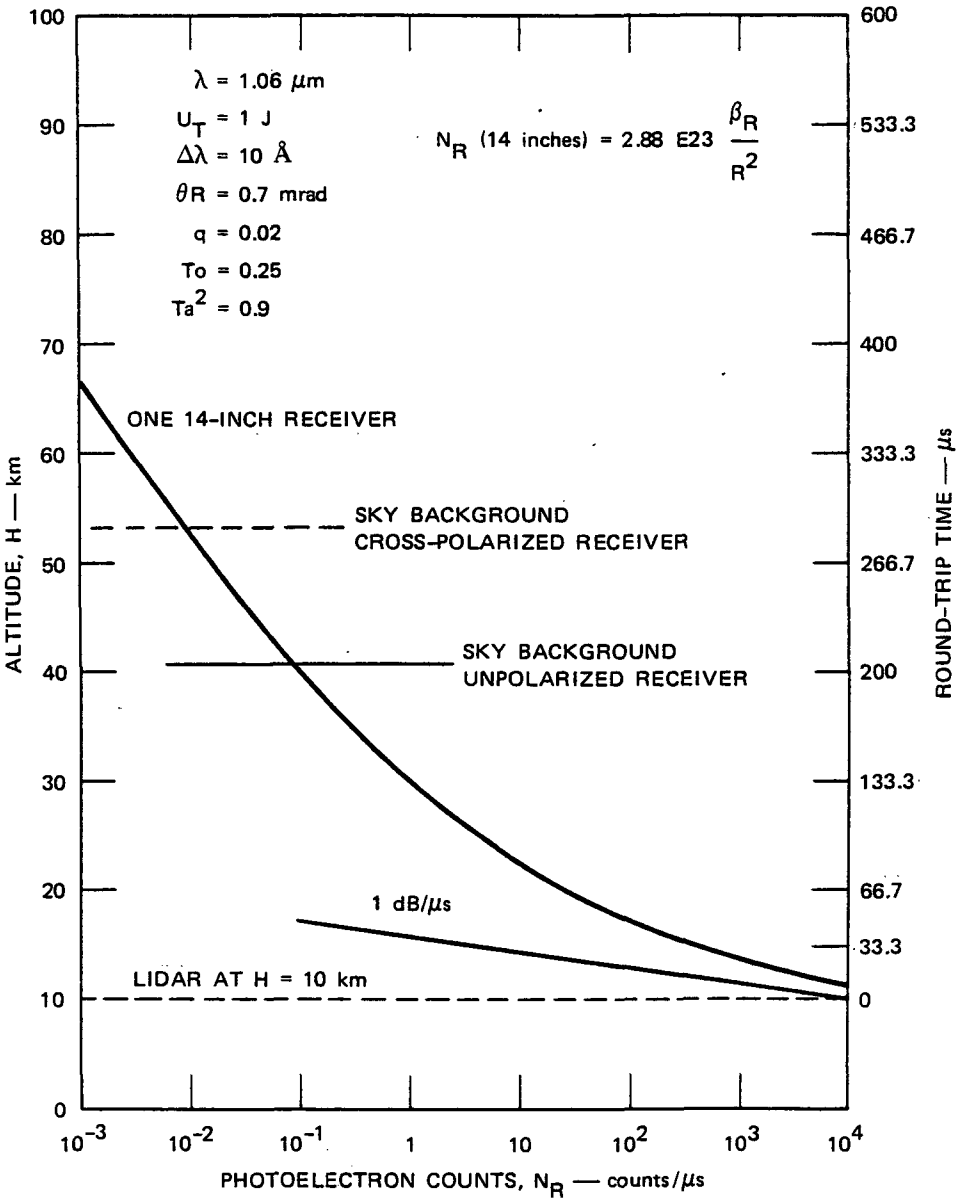

FIGURE 12 PREDICTED SIGNAL RETURN RESULTING FROM RAYLEIGH MOLECULAR BACKSCATTER — Nd SYSTEM

Table 1

ASSUMED LIDAR SYSTEM PARAMETERS

Symbol	Definition	Value	Units
U_T	Radiated transmitter, energy per pulse (pulse length << integration period)	1	J
A_R	Receiver effective aperture area. Includes effect of mechanical aperture blockage but not of optical transmission factors	0.080 (d = 0.32 m)	m^2
T_O	Receiver optical transmission factor. All components in tandem.	0.25	--
λ	Wavelength	1.06 E-6	m
q	Detector quantum efficiency at wavelength λ	0.02	--
Ω_R	Receiver angular field of view	$\frac{\pi}{4}$ (0.5)E-6	sr
$\Delta\lambda$	Optical filter bandwidth	10	Å
β_R	Rayleigh volume backscatter coefficient	3E-8 (h = 11 km, λ = 1.06 μm)	m^{-1} sr^{-1}

The light excitation used in the first test was sufficient to generate 1.25×10^4 photoelectrons per microseconds, which for a tube gain of $G = 10^6$ yields an anode output pulse of 100 mV into 50 ohms. The pulse length was 10 μs. The anode count rate obtained at the end of various time intervals after onset of the exciting pulse was then measured using a gated counter. In all cases the gate "on" time was 10 μs and the pulse repetition rate was 48.6 Hz. Average count rates for the various bins were determined by accumulating counts for 10 or 20 s, yielding sampling periods of 4,860 or 9,720 μs, the longer period being used for very low signal levels.

Initial tests revealed that a measureable noise increase was indeed present, but they also uncovered an instrumentation problem that should not be overlooked in lidar receiver design. With the tube gain set high enough ($G + 10^6$) to permit photon counting, the amplified analog signal from the simulated near-lidar atmospheric return was strong enough not only to saturate the photon counting preamplifier, but also to completely paralyze it for a period of some 90 μs after termination of the pulse. To avoid the saturation, the exciting pulse level was reduced approximately 13 dB and the data reproduced in Figure 13 were taken. Comparison of the noise resulting from even this reduced level with the expected signal returns (Figure 12) reveals that the effect cannot be summarily ignored. For example, the noise level is greater than one percent of the expected signal amplitude for all measurement altitudes above about 30 km.

Next, an attempt was made to reduce the tube gain during the strong signal period by employing the dynode modulation technique described earlier. While the trend was in the predicted direction--the paralysis effect was reduced and the induced noise level remained fairly high--reliable data were never obtained in this mode because of a strong proclivity of the test setup to oscillate or be influenced by ambient radio frequency radiation. It was apparent that improved shielding by-passing and comnent layout would be required for successful simultaneous operation of both the high-gain pulse-counting preamplifier and the circuitry for dynode modulation. The solution adopted for the remainder of the induced-noise tests was to shunt the input to the preamplifier with a shorted stub transmission line--a 6-ft length of 50-ohm coaxial cable shorted at the far end. This permitted the high-frequency "single photon" pulses to pass, but prevented buildup of any appreciable analog voltage.

A further change was to use, as a exciting light source, a pulse waveform that was more representative of the energy distribution in an actual lidar return than was the rectangular pulse used for the first test. This was obtained by adding a 0.07-μF capacitor in series with the LED light source. This capacitor, in concert with the total series resistance in the circuit, produced a light pulse with a very

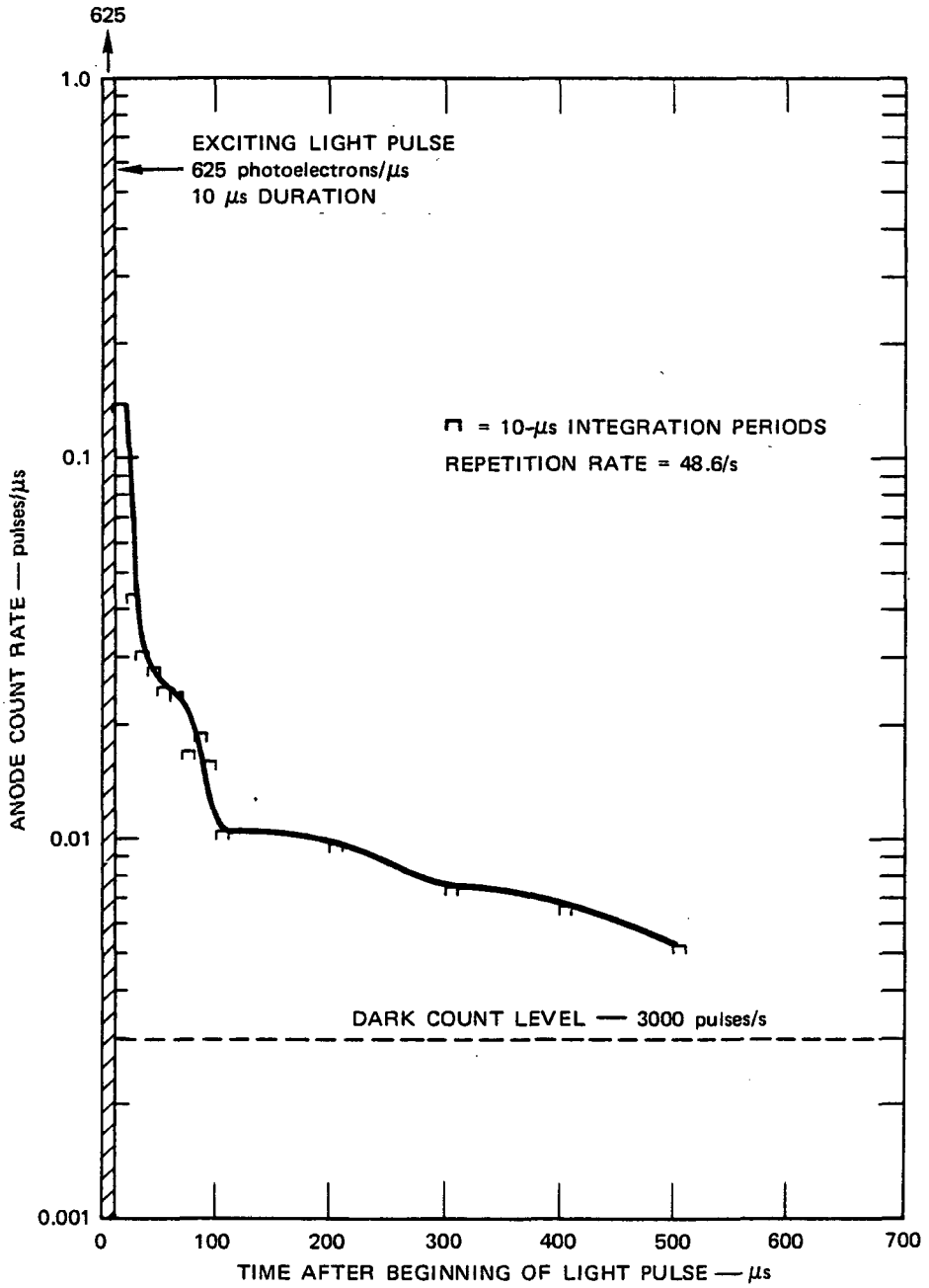

FIGURE 13 SIGNAL-INDUCED NOISE FROM 10-μs RECTANGULAR LIGHT PULSE — VPM-164A, SERIAL NO. 082, DATA TAKEN FEBRUARY 17, 1978

uniform exponential decay of 1 dB/μs. The pulse decay was observed to be linear over a range in excess of five decades by monitoring with a separate PMT and logrithmic amplifier setup.

The data suggest, but do not completely provide irrefutable evidence, that the light output continues to decay at least as rapidly as 1 dB/μs for the next approximately four decades required for the detector response to be well below the background noise level. Furthermore, it is not known for sure whether possible fluorescence within the optical components will affect this decay rate at very low levels. However, Pettifer did test for these effects using a rotating mechanical shutter and found them to be insignificant.

Figure 14 shows the results obtained with the exponential pulse for two peak levels; the upper curve corresponds approximately to the peak return expected when looking upward from 10 km, and the lower curve is for a peak amplitude 15.4 dB less.

For the larger pulse, the total integrated number of cathode photoelectrons released would be 5.43×10^4, or about 8.7 times the total number released by the rectangular pulse used for Figure 13. This test indicates that an induced noise level of one percent of the expected Rayleigh signal level might be expected for measurement altitudes above about 20 km. Thus it would appear desirable to attempt to characterize this effect more completely than has been done here, so that appropriate corrections can be included during analysis of lidar data.

H. Single-Electron Statistics

In Figure 15, Curves (a) and (b) are reproduced from Ref. 1 and show two pulse amplitude distributions indicating that appreciably improved single electron statistics had been demonstrated with multiplier sections employing a gallium phosphide (GaP) semiconductor as the first dynode element, as compared to the performance of similar structures employing the more usual beryllium copper (BeCu) for all dynode elements. These data had been obtained from the VPM 164A manufacturer during the 1977 lidar design study reported upon in Ref. 1.

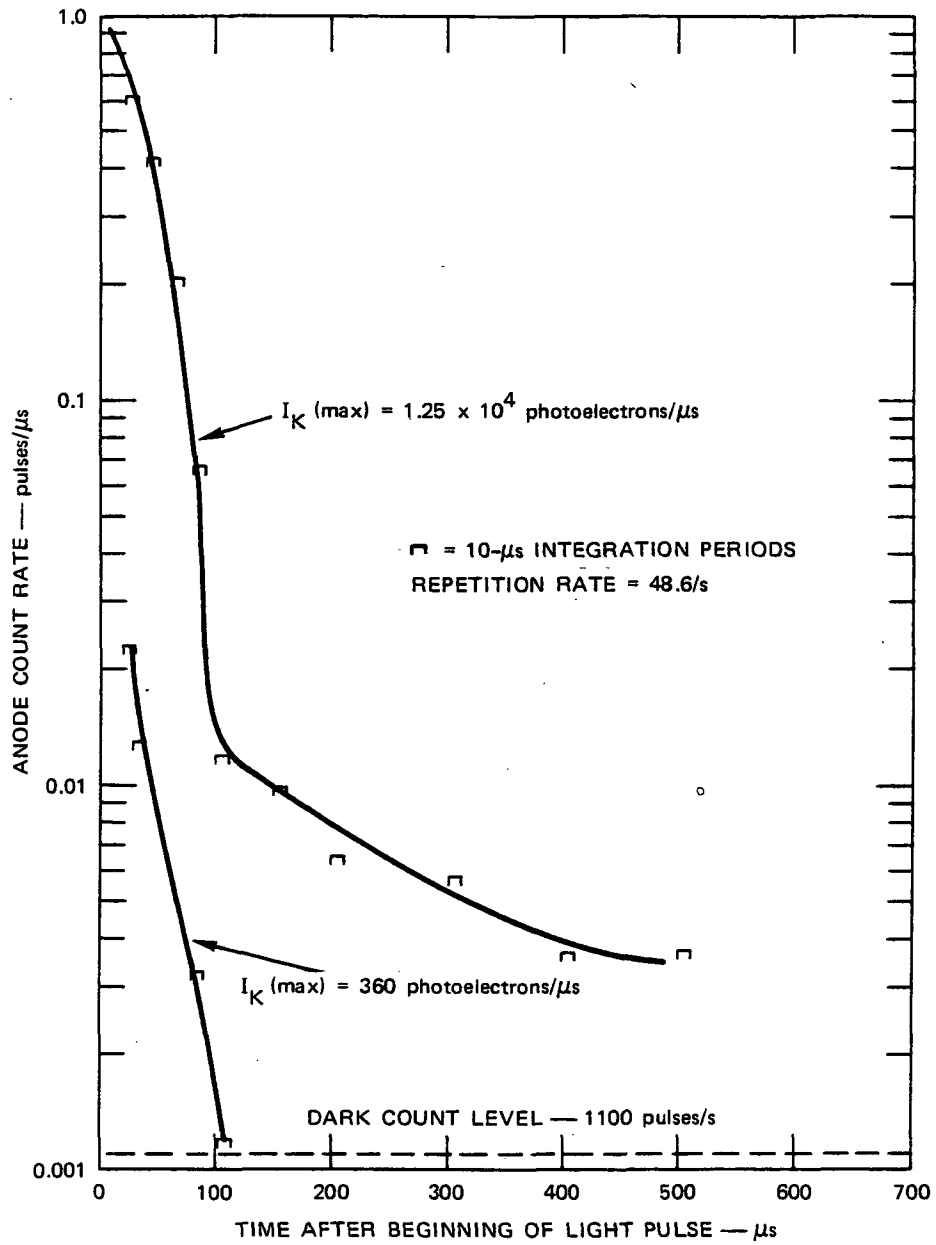

FIGURE 14 SIGNAL-INDUCED NOISE FROM LIGHT PULSE WITH EXPONENTIAL DECAY — VPM-164A, SERIAL NO. 082, LIGHT DECAY SLOPE = 1 dB/μs, DATA TAKEN MARCH 7, 1978

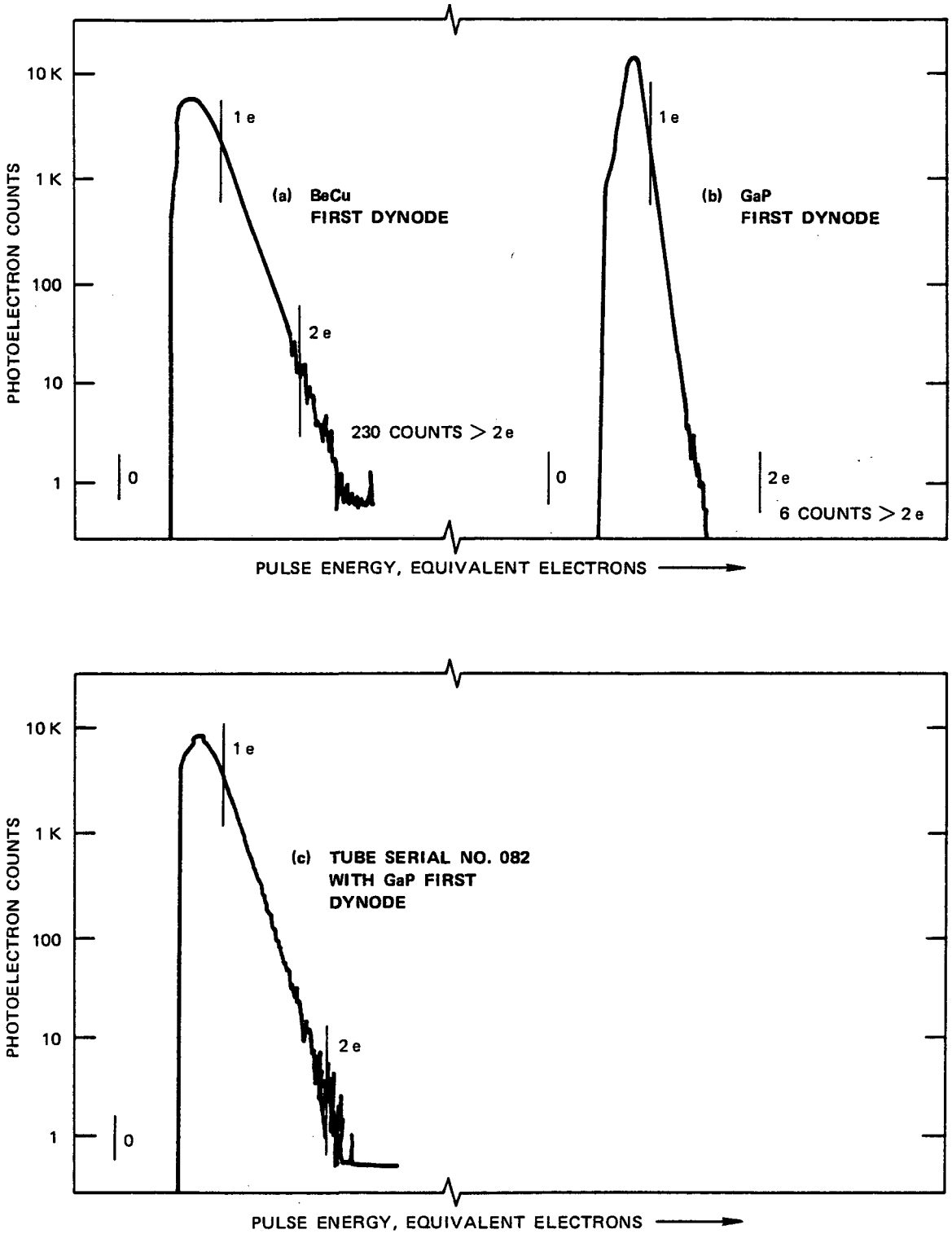

FIGURE 15 PULSE HEIGHT DISTRIBUTIONS FROM VPM-164A PMT, SERIAL NO. 082 COMPARED TO PREVIOUS SAMPLES

In seeking the best available state-of-the-art detector performance for possible application in the airborne stratospheric lidar, the evaluation PMT was ordered with the GaP first dynode option. Curve (c) of Figure 15 shows that the amplitude distribution actually achieved in the delivered tube (Serial No. 082) is almost identical to that previously shown for the BeCu structure [Curve (a)]. The data for Curve (c) were taken from a chart record made on tube 082 four days before delivery, using the same pulse-height analyzer equipment that had generated the other two curves. An essential duplicate of Curve (c) was also obtained at SRI by plotting the derivative of the cumulative amplitude distribution obtained by progressively lowering the counting threshold.

The discrepancy has been only very briefly discussed with a technical representative of the manufacturer, who pointed out that tubes are not yet specified to yield any particular amplitude distribution. It is not yet clear how representative tube No. 082 is of its class, or in fact, how feasible it is to define a quantitative measure of the lidar system improvement that might accrue from a narrower distribution.

The discussion revealed that the very steep falloff on the left side of all curves in Figure 15 results from a lower-bound threshold setting in the pulse-height analyzer equipment, not from a lack of pulses with low amplitudes. It was stated that this lower threshold normally is set in the region of 0.25 to 0.33 electron equivalents (3).* This is primarily for the reason that the greatest interest for previous pulse-counting applications has been in the right-hand side of the curve (to obtain good discrimination between one- and two-photon events); a secondary reason results from the difficulty of obtaining reliable data at very low amplitudes.

For the lidar application, the left half probably is more important because a steep falloff on the left is desirable to discriminate between true photocathode events and other sources of anode output. A steep slope on the left is desirable to facilitate setting a reliable and repeatable discriminator level.

---

* See footnote in Section III-F.

This whole question will need more attention in order to effect the desired smooth transition between analog and pulse-counting modes in the proposed lidar.

I. Miscellaneous Operating Considerations

1. DC Limitations

It should be axiomatic that the lidar will require either automatic shuttering or rigorous operating precautions to prevent direct viewing the sun or viewing close to the sun through haze or thin cloud. It is also worthwhile to examine the possible consequences of prolonged viewing of bright sunlit clouds. A typical value for the radiance of such clouds in the wavelength region of 1.06 μm is 0.014 W m^{-2} sr^{-1} $Å^{-1}$.* When applied to a receiving system having a 2-mrad field of view and other parameters as previously listed in Table 1, the cathode illumination is found to be:

$$P_{dc} = 8.80E\text{-}9 \text{ W} \quad .$$

For a cathode sensitivity of 35 mA/W (per curve in the Appendix) the resulting cathode current would be:

$$I_k = 3.08E\text{-}10 \text{ A} \quad .$$

While this value is comfortably below the specified limit of 100 nA for cathode current, the 1-μA limitation for anode current would be exceeded for any tube gain in excess of 3.3×10^3. Since gains two to three decades higher will be required during normal operation, the need for dynamic gain control or optical shuttering is apparent.

2. Upper Frequency Limit for Pulse Counting

The anode current pulses resulting from a very low level of cathode illumination were observed with a 500-MHz oscilloscope preceded

---

* See, for example, Figure 5-1 of Ref. 5.

by the same wideband preamplifier (rise time = 6 ns) used for pulse-counting tests. For a PMT gain of 10^6, the half-amplitude pulsewidth was observed to be 20 ns. This broadening due to transit-time dispersion in the multiplier chain will limit pulse counting by normal techniques to average rates less than 5 to 10 MHz. For the airborne lidar system whose performance was plotted in Figure 12, pulse counting would be reserved for altitudes above 22 to 25 km, and some means of charge integration will be needed for lower altitudes.

3. More About Dynamic Range

It should be pointed out that if the tube is operated with a gain of 10^6 as it was for these tests to achieve a reasonably high signal level for interfacing to the pulse-counting circuitry, then there remains only a little more than three decades of useful analog dynamic range between the 10-pulse-per-microsecond count rate discussed above and the region of severe anode current saturation reported in Section III-D (2 mA of anode current corresponds to 12,500 pulses per microsecond at the cathode). The use of dynamic gain control is probably the most powerful single method of extending the useful dynamic range. In addition, consideration should be given to other measures that might help. One possibility would be to attempt to raise the level of anode current saturation through the use of a tapered voltage divider string instead of the linear one employed here. Interfacing to the pulse-counting preamplifier at a lower signal level would also help if it were carefully done to avoid oscillation or RF pickup. That is, external amplifier gain could be exchanged for PMT gain.

IV CONCLUSIONS

The tests performed and the valuable discussions with factory representatives afforded by this evaluation indicate that the VPM-164A photomultiplier is a suitable candidate for use in an airborne stratospheric lidar operating at 1.06 μm wavelength.

For high-performance applications, the remarkably high quantum efficiency (4.3% for the tested sample; 2 to 6% for the tubes as a class) provides adequate compensation for the additional design and maintenance care required to use the tube. That additional care will include: (1) providing moderate cooling both during operation and storage, (2) coping with the dynamic range limitations imposed by a relatively low anode current before saturation, and (3) providing some form of light shuttering during standby and interpulse periods to prevent cathode damage from high sustained levels of incident light.

The tube absorbs large pulse overloads without apparent serious impairment of subsequent analog performance. However, the internal noise level does appear to rise significantly following even very modest pulsed illumination, and this characteristic needs more study.

It is not clear that the addition of the gallium phosphide first-dynode option guarantees sufficient advantage in pulse-counting performance to compensate for the cost premium, typically longer procurement time, and reduced availability of samples from which to select for high cathode efficiency.

"Page missing from available version"

Appendix

MANUFACTURER'S DATA SHEETS FOR VPM-164A PHOTOMULTIPLIER

"Page missing from available version"

DATA SHEET FOR TUBE SERIAL NUMBER 082 (Cathode Quantum Efficiency, Multiplier Gain, and Anode Dark Current)

Device Type · VPM-164A.12SPL
Serial Number · 082

Designation ·
- Number of Dynode Stages · 12
- Cathode Type · InGaAsP
- Window Material · Sapphire

Ratings
- Operating Voltage · -1800 VDC Nominal
- Bleeder Impedance · 10 M ohm K to D1 & D1 to D2, 5 M ohm/stage D2 thru D12 to G.R.
- Cathode Current · 100na. Max.
- Lead Designation · See attached drawing for lead designation

Performance

Sensitivity:

Luminous 2870° K ·
5113 Filter ·
2540 Filter · 120ua/hℓ

* Radiant	· 5,300	Å	84.0	mA/watt	19.6	%QE See attached QE curve
	· 10,600	Å	37.0	mA/watt	4.3	%QE
	· 11,000	Å	8.4	mA/watt	.95	%QE

*Gain/Dark Current

1 x	10^4 Gain at	-1085	volts with	DKI
1 x	10^5 Gain at	-1433	volts with 5.0^{-10}A	DKI
1 x	10^6 Gain at	-1880	volts with	DKI
	10^7 Gain at		volts with	DKI

Remarks:
1. Connect "K" & "D1" leads together to a negative high voltage power supply (-2000 VDC Max.), and ground "G.R." lead for normal DC operation.
2. Output signal appears @ "C" lead.
3. All remaining leads must be insulated properly at all times when not in use.
4. CAUTION ! Window flange is at Dynode 1 potential (-2000 VDC Max.) during operation.
5. Maximum average anode current, 1ua.
6. Maximum storage and operating temp., -20°C.
7. Minimum storage and operating temp., -100°C.
8. Dark current incrases linearly with QE @ 1.06u.

by R.W. Moffett date 2/3/78

* = Data taken @ -20°C

SPECTRAL SENSITIVITY CURVE FOR TUBE SERIAL NUMBER 082

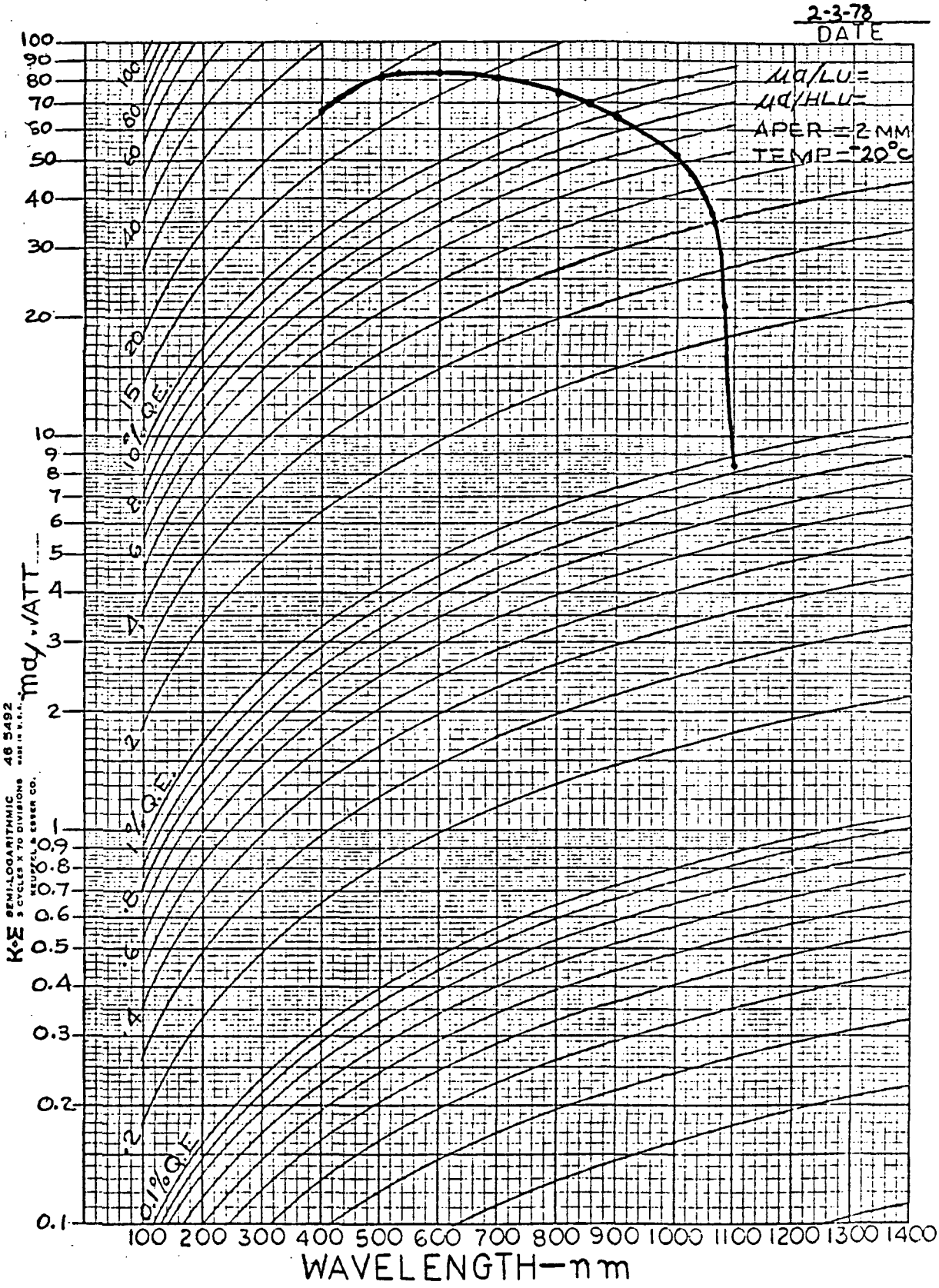

WIRING DIAGRAM AND COLOR CODE

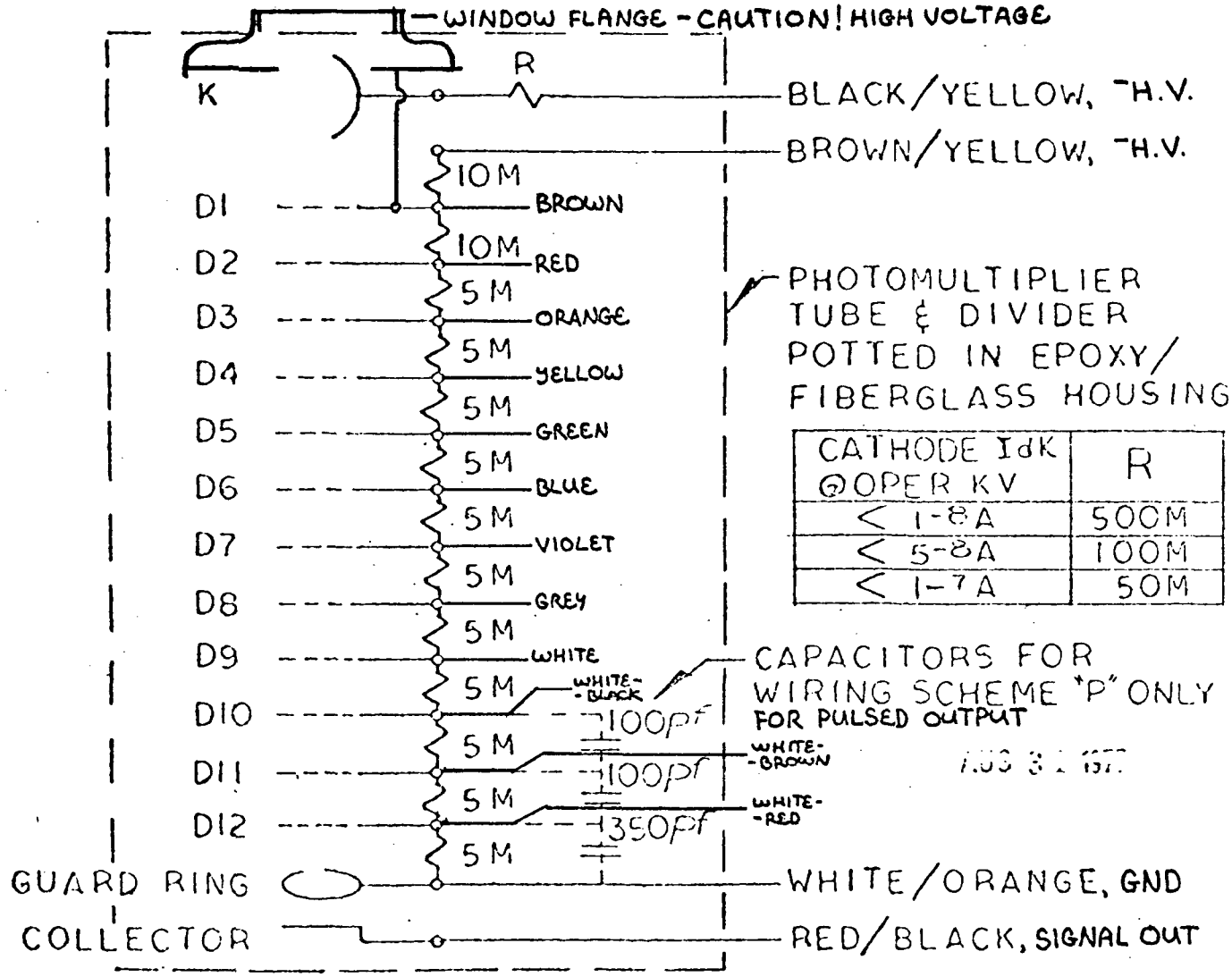

CATHODE IdK @OPER KV	R
< 1-8A	500M
< 5-8A	100M
< 1-7A	50M

QTY	IDENTIFYING NUMBER	DESCRIPTION	CODE IDENT	ITEM

LIST OF MATERIALS

UNLESS OTHERWISE SPECIFIED DIMENSIONS ARE IN INCHES
DEC. 1PL ± .1 2PL ± .02
3PL ± .005 FRAC ± 1/64
ANG ± 1° SUR √
MATERIAL
SPEC NO.
FINISH

CONTRACT NUMBER

DR	CAPCOM	2-2-77
CHK	[illegible]	2-3-77
APPD	[illegible]	2-4-77
APPD	[illegible]	2-7-77

DESIGN ACTIVITY APPROVAL 2-3-77
CUSTOMER APPROVAL

varian

LSE

PMT WIRING SCHEME D&P
VPM-164 SERIES W/DIVIDER

SIZE	CODE IDENT NO.		
A		VPM 164A.12 SPL #082	C

SCALE CLASS 'B' SHEET OF

varian

PRELIMINARY
TECHNICAL DATA

VPM-159, VPM-164
Series

III-V 12-STAGE
UV TO NEAR IR
PHOTOMULTIPLIERS

FEATURES

- Solid State III-V photocathodes — three types
- High quantum efficiency (QE)
- Broad spectral response -- 145 to 1100 nm
- Computer-designed optics for high gain and low dark current
- Rugged, ultra-high-vacuum, metal-ceramic envelope
- Anode guard ring construction
- Integral voltage divider
- Precision vacuum encapsulation
- Operable in ambient environments from +20 to -195° C

DESCRIPTION

The VPM-159 and VPM-164 series are III-V, 12-stage UV to near IR photomultipliers for use in astronomy, spectroscopy, high-resolution densitometry, photometry, spectrometry, scintillation counting, electro-optical countermeasures, multiple-wavelength laser detection up to 30 megahertz, and other low and very-low light-level detection applications.

The VPM-159 series are equipped with a one-half-inch diameter side window and the VPM-164 models employ three-quarter-inch end-window construction. Each window is synthetic sapphire (145 nanometer cutoff), aligned with its photocathode. Special windows having a cutoff of 112 nanometers can be furnished.

Photocathodes are state-of-the-art III-V InGaAsP (A series), GaAs (M series) or GaAsP (S series) front-surface emitters for broadband UV to IR radiation detection. Optional devices are available for X-ray detection.

The rugged metal-ceramic envelope incorporates a low-excess-noise, electron-optically-focused, beryllium-copper, venetian-blind dynode structure. For the ultimate in quantum efficiency and low dark current performance, the end-window (VPM-164) models can be furnished with a gallium phosphide (GaP) first dynode instead of beryllium copper (BeCu) to provide extremely high secondary emission ratios and improved gain statistics for counting use.

Biasing is simplified by the integrated voltage divider of precision, high-reliability resistors welded to the metal dynode flanges. For pulse detection, an optional R-C circuit is available to prevent undesirable voltage-divider loading.

A fiberglass housing and encapsulation material, matched to the application, seal the tube envelope completely to maintain a stable, low-leakage-current environment. Tube connections are made safely and easily by means of insulated flying leads or optional tube sockets. Optional RFI-EMI shields are also available.

Dark current and dark count rate can be decreased dramatically by operating these photomultipliers at reduced temperatures such as -20° C (thermoelectric cooling), -50° C (refrigeration cooling), -78° C (dry ice cooling), -100° C (regulated liquid nitrogen cooling), or, for lowest dark current, -195° C (submersion in liquid nitrogen) in a non-encapsulated configuration ideal for photon counting.

3631 2/77

Printed in U.S.A.

GENERAL CHARACTERISTICS [1,4]

ELECTRO-OPTICAL

Photocathode[2]	
Quantum Efficiency	See Figure 1
Anode Sensitivity, S_A	
at 10^5 gain	See Figure 2
Equivalent Noise Input, ENI	
at -78°C	See Figure 3
Anode Dark Current, I_d (Dark Noise), [3,5]	
at 10^5 current amplification	See Figure 4
Excess Dynode Noise, at 10^5 gain	
BeCu	< 2 dB
GaP	< 1 dB
Current Amplification (Gain, G) typical	
At -1300 Vdc	10^4
At -1700 Vdc	10^5
At -2400 Vdc	10^6
On Request	10^7
Average Anode Current, max	1 μA
Pulse Anode Current	
1% duty, max	100 μA
Rise Time, 10 to 90%	10 ns
Decay Time, 10 to 90%	20 ns
Modulation Bandwidth	30 MHz
Maximum Operating Voltage	
VPM-159 series	-3000 Vdc
VPM-164 series	-3500 Vdc
Voltage Divider Current Requirements, max	
at -2400 Vdc	330 μA

PHYSICAL

Dimensions[6]	See Outline Drawings
Weight	
VPM-159 Series	0.5 lb/227 g
VPM-164 Series	1.0 lb/454 g
Mounting Position	Any
Connection	Four Flying Leads
Materials	
Photocathode	
VPM-159A & VPM-164A	Indium Gallium Arsenide Phosphide
VPM-159M & VPM-164M	Gallium Arsenide
VPM-159S & VPM-164S	Gallium Arsenide Phosphide
Window	
Standard	Sapphire (No = 1.77)
Optional	Magnesium Flouride, UV Grade Sapphire, Lithium Flouride, or Quartz
Dynodes	
Standard	BeCu Alloy
Optional, first dynode, VPM-164 Series, see Figure 5	GaP

ENVIRONMENTAL

Temperature Range, storage and operating[7]	
Standard Configuration	-78 to +20 °C
Optional Configuration	-100 to +20 °C
Unencapsulated	-195 to +20 °C

OPERATING HAZARDS

Read the following and take all necessary precautions to protect personnel. Safe operating conditions are the responsibility of the equipment designer and the user.

High Voltage. This tube operates at voltages which can be deadly. Equipment must be designed so personnel cannot come in contact with operating voltages. Enclose high-voltage circuits and terminals and provide fail-safe interlocking switch circuits to open the primary circuits of the power supply and to discharge high-voltage capacitors whenever access is required.

Equipment must be designed to fully safeguard all personnel from these hazards. Labels and caution notices must be provided on equipment and in manuals clearly warning of those hazards which cannot be avoided.

NOTES:

1. Characteristic values are typical and are based on performance tests. These figures may change without notice as the result of additional data or product refinement. Consult Varian LSE before using this information for final equipment design.
2. The InGaAsP photocathode can be tailored for individual applications to optimize quantum efficiency at a specific wavelength and ambient temperature between room temperature and -195°C. As an option, the long wavelength cutoff limit can be extended to 1150 nm.
3. Dark current is measured with zero photocathode illumination.
4. When ordering, specify quantum efficiency, wavelength, dark current and ambient temperature required.
5. Dark current performance is a function of photocathode material, envelope type, and ambient temperature. Achievable dark count rates range from less than one (1) to 100 counts per second, with the VPM-164S having the lowest count rate and the VPM-159A having the highest. As with anode dark current, dark count performance improves inversely with temperature.
6. Optional configurations are available. They include (1) smaller diameter housing, (2) housings with pins, (3) housings with pins and sockets (external voltage divider), (4) unencapsulated for -195°C operation (with or without voltage divider).
7. "M" and "S" photocathodes can be fabricated for higher temperature operation on request.

CHARACTERISTIC CURVES

Typical performance values

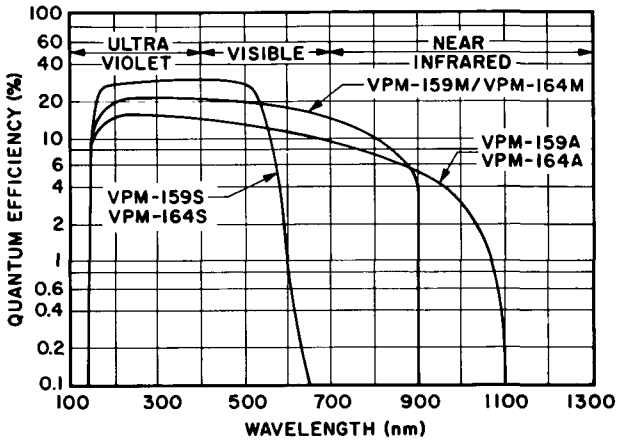

Figure 1

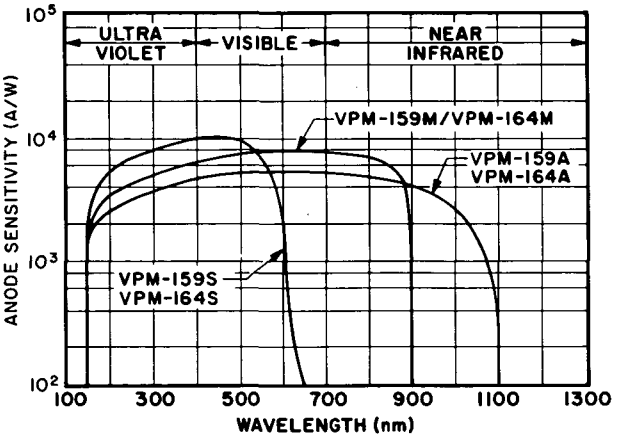

Figure 2

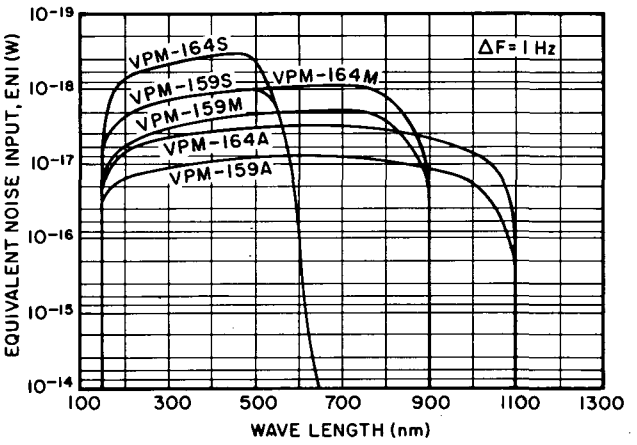

Figure 3

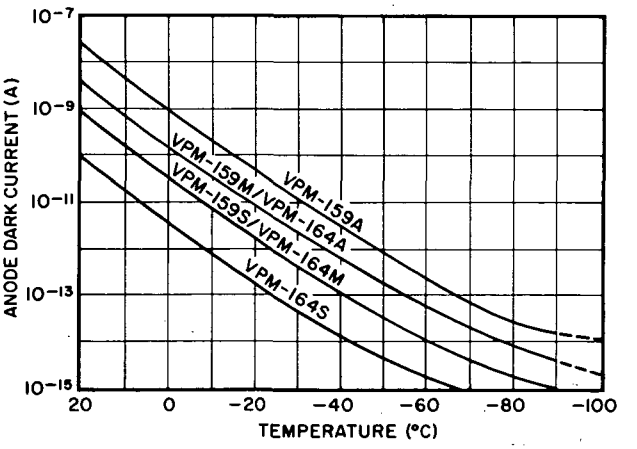

Figure 4

$$ENI = \frac{(2e\,Id\,\Delta f\,G)^{1/2}}{S_A}$$

WHERE

ENI = EQUIVALENT NOISE INPUT IN WATTS
e = ELECTRONIC CHARGE OF 1.6×10^{-19} COULOMBS
Id = ANODE DARK CURRENT AT GAIN G
Δf = 1 HERTZ BANDWIDTH, UNLESS OTHERWISE SPECIFIED
G = TUBE GAIN (CURRENT AMPLIFICATION)
S_A = ANODE SENSITIVITY AT GAIN G IN AMPERES/WATT

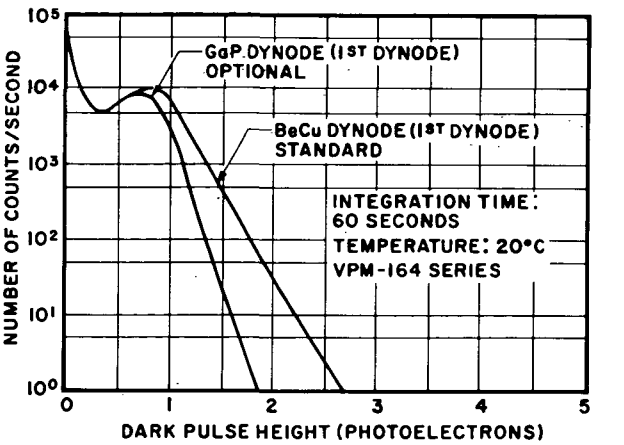

Figure 5

OUTLINE DRAWINGS

VPM-159 Series

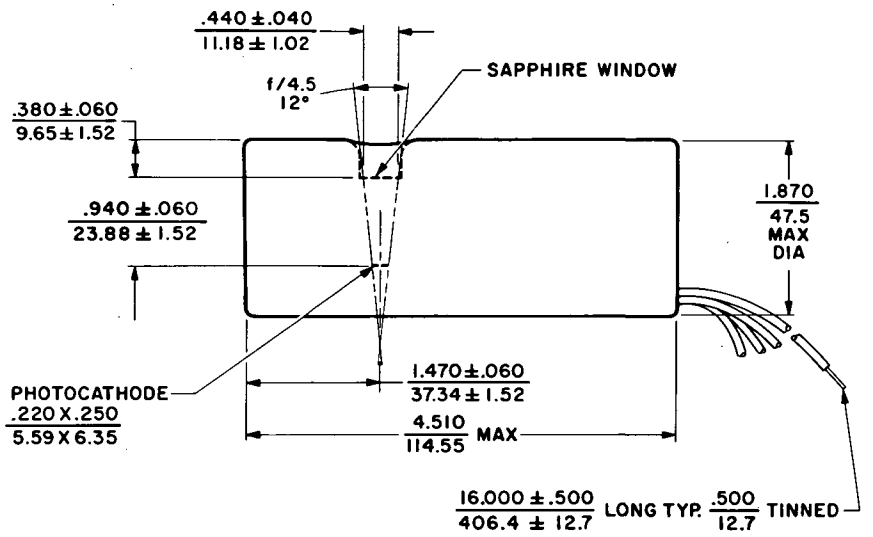

VPM-164 Series

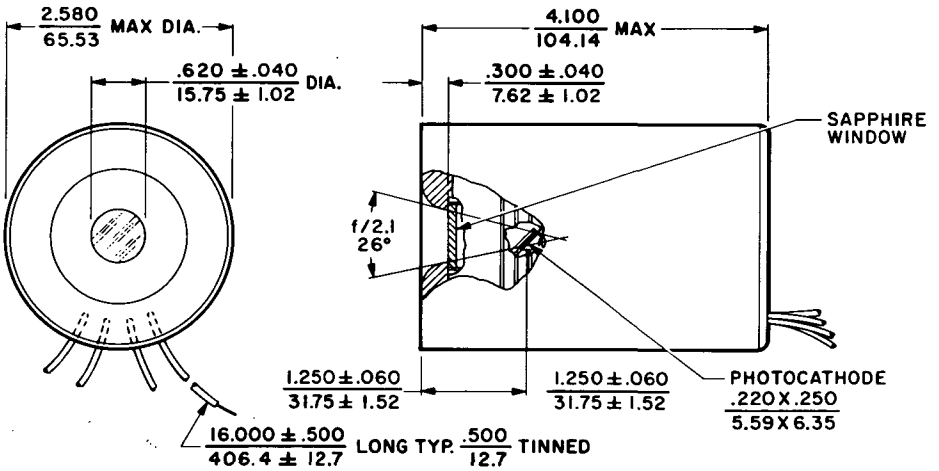

LEAD CONNECTIONS	
RED/BLACK	ANODE
WHITE/ORANGE	GUARD RING
BROWN/YELLOW	DIVIDER STRING
BLACK/	PHOTOCATHODE

DIMENSIONS: ← inch / mm →

"Page missing from available version"

varian LSE / 601 california avenue / palo alto / california 94304 / u.s.a. / 415 / 493-4000

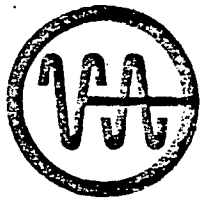

VARIAN LSE STANDARD WARRANTY

All Phototubes manufactured by Varian LSE are warranted to be free from defects in material and workmanship for 100 hours of operation or 90 days from date of original shipment, whichever occurs first. This Warranty is in lieu of and excludes all other express or implied warranties of merchantability or fitness or otherwise. This Warranty does not extend to any tube which in the opinion of Varian LSE, has been subjected to misuse, neglect, accident, operation outside the tube's maximum ratings, incorrect wiring, improper installation, use in violation of instructions furnished by Varian LSE or which has had its serial number or any part thereof altered, defaced or removed. Under no circumstances will Varian be liable for incidental or consequential or resulting loss or damages of any kind whatsoever, howsoever caused.

In any event Varian LSE's obligations under this Warranty will not in any way extend beyond the original purchase price paid for the tube. In addition Varian LSE shall have sole discretion with regard to refund or replacement if any adjustment is awarded by Varian LSE.

7/8/74

varian LSE / 601 california avenue / palo alto / california 94304 / u.s.a. / 415 / 493-4000

SHIPPING, HANDLING, AND OPERATING INSTRUCTIONS FOR VARIAN LSE PHOTOMULTIPLIER TUBES

INTRODUCTION

This information is provided to the photomultiplier tube (PMT) user to enhance trouble-free operation of the device. Although these PMT's are of a rugged ceramic-to-metal seal design, certain precautions must be taken to protect the tube and photocathode material and thus to achieve optimum operation. PMT performance is directly related to the shipping, handling and operating history.

SHIPPING/STORAGE

1. Every PMT having a solid-state III-V material photocathode is shipped to the buyer in a dry-ice packed container to preclude damage caused by high ambient temperatures. This package will protect the PMT from the affects of normal shipping temperatures for three (3) days from the date of shipment from Varian LSE. By the end of said three (3) day period, the buyer must remove the PMT from the shipping container for storage in an area having controlled ambient temperatures between +20°C (70°F) and -78°C (-172°F).

2. In the event that subsequent shipping of the III-V PMT is required, care should be taken to repack the shipping container with enough dry-ice to protect the device during shipment. When shipping a tube to Varian LSE, it must be packaged in the original shipping container or in a suitable alternative container packed with dry-ice. Varian LSE must be notified of the time and place of return shipment prior to that shipment.

HANDLING

1. Handle the device by the housing only. DO NOT hang from or pull by the flying leads.

2. When cleaning the window, always use normal lens cleaning techniques for washing and wiping. More harsh cleaning methods could scratch the window material.

3. Unless specified otherwise, DO NOT subject the tube to shock greater than 10 g's or temperature variations greater than 20°C/hour.

OPERATION

1. Be sure that the cathode lead is connected to the internal voltage divider circuit, and apply negative voltage to both of these leads. Wiring instructions are given with the tube data sheet.

2. During initial turn-on, monitor the tube anode current while increasing either tube voltage or photocathode irradiance. Be careful not to exceed the specified maximum continuous anode current. Once assured that the circuit is accurately connected and that the anode output current is safely ascertained, voltage to the PMT can be turned on and off without damage at any voltage up to the maximun specified on the tube data sheet.

3. From time to time, check the applied voltage, anode current, and ambient temperatures to be sure that each is within the limits of the PMT specification. It is advisable, to ensure extended tube lifetime, that all PMT's having III-V photocathodes be stored and operated at or below -20°C. For storage purposes, a commercially available freezer will maintain this temperature.

4. When in doubt about the operating requirements of this PMT, please feel free to call Varian LSE at (415) 493-4000 ext. 3502. Ask for Photomultiplier Tube Applications or Production Engineering.

October 30, 1974

QUANTUM EFFICIENCY WARRANTY

Varian LSE warrants that the quantum efficiency (Q.E.) of the accompanying phototube will not degrade below the minimum specified value for a period of one (1) year from date of original shipment when said phototube has been continuously stored and operated between the temperature limits of -20°C and -78°C, provided that all the terms and conditions of the attached phototube Standard Warranty have been complied with. Should Q.E. degrade below the minimum specified value within said one (1) year period, the Buyer, at his option, may return the phototube to Varian LSE for adjustment. Varian LSE, at its sole discretion, shall make one of the following adjustments on any phototube returned under this Quantum Efficiency Warranty:

(1) Repair said phototube by restoring the Q.E. to at least the minimum specified value.

(2) Replace said phototube with a phototube having a Q.E. of at least the minimum specified value.

(3) Issue a credit as follows:

Any credit under this Q.E. Warranty shall be limited to the original purchase price paid for said phototube for the first three (3) months from the date of original shipment, and shall thereafter be linearly prorated for the remaining nine (9) months.

Any repair or replacement under (1) or (2) above shall be subject to a charge not to exceed the original purchase price paid for said phototube less the amount of credit due under (3) above. Further, any repaired or replaced phototube shall carry the unused portion of the Warranty remaining on the original phototube. In any event, Varian LSE's obligations or liabilities under this Q.E. Warranty shall not in any way extend beyond one (1) year from the date of original shipment nor extend beyond the original purchase price.

REFERENCES

1. W. E. Evans, "Design of an Airborne Lidar for Stratospheric Measurements," Final Report, Contract NAS1-14520, Stanford Research Institute, Menlo Park, Calif., NASA CR-145179 (1977).

2. R. J. Allen and W. E. Evans, "Laser Radar (LIDAR) for Mapping Aerosol Structure," Rev. Sci. Instr., Vol. 43, No. 10, p. 1422 (October 1972).

3. R. E. W. Pettifer, "Signal Induced Noise in Lidar Experiments," J. Atmos. Terr. Phys., Vol. 37, pp. 669-673 (1975).

4. R. E. W. Pettifer and P. G. Healey, "Signal Induced Noise in a 56 TUVP Photomultiplier," J. Phys. E: Scientific Instruments, p. 617 (1974).

5. Handbook of Military Infrared Technology, Office of Naval Research, Department of the Navy, (U.S. Government Printing Office, Washington, D.C., 1965).

6. W. H. Hunt, "Measurements of Signal-Induced Noise in Photomultipliers in a Lidar System," presented at the Seventh International Laser Radar Conference, Menlo Park, Calif. (November 4-7, 1975).

"Page missing from available version"

LIBRARY CARD ABSTRACT

A high-performance near-infrared-sensitive photomultiplier tube was procured and evaluated with emphasis on those characteristics affecting its use over the very large amplitude range of signals encountered by an airborne lidar intended for mapping the distribution of stratospheric aerosols.

A cathode quantum efficiency of 4.3% at 1.06 μm wavelength and a background count of less than 10,000 per second were realized. It is recommended that the tube be stored and operated at a temperature near -20°C, or cooler. Performance was found acceptable for the application in both pulse-counting and analog modes, but careful design, probably including dynamic gain control, will be required to effectively utilize both modes on the same lidar shot.